Identification of essential genes that support fitness of *Acinetobacter baumannii* efflux pump overproducers in the presence of fluoroquinolone

Efrat Hamami[1], Wenwen Huo[1], Katherine Neal[3], Isabelle Neisewander[1], Edward Geisinger[1,2], Ralph R. Isberg[1,*]

[1]Department of Molecular Biology and Microbiology, Tufts University School of Medicine, 150 Harrison Ave., Boston, MA 02111, USA.

[2]Department of Biology, Northeastern University, Boston, MA, 02115, USA

[3]Department of Biochemistry, Curry College, Milton, MA, USA.

[*]Corresponding Author

Abstract

Acinetobacter baumannii is a nosocomial pathogen often associated with multidrug resistance (MDR) infections. Fluoroquinolone resistance (FQR) due to drug target site mutations and elevated expression of RND drug transporters is common among clinical isolates. We describe here a CRISPRi platform that identifies hypomorphic mutations that preferentially altered drug sensitivity in RND pump overproducers. An sgRNA library against essential genes of *A. baumannii* was constructed with single and double nucleotide mutations that produced titratable knockdown efficiencies and introduced into multiple strain backgrounds. Other than *nusG* depletions, there were few candidates in the absence of drug treatment that showed lowered fitness specifically in strains overexpressing clinically relevant RND efflux pumps AdeAB, AdeIJK, or AdeFGH. In the presence of ciprofloxacin, the hypomorphs causing hypersensitivity were predicted to result in outer membrane dysfunction, to which the AdeFGH overproducer appeared particularly sensitive. Depletions of either the outer membrane assembly BAM complex, LOS biogenesis proteins, or Lpt proteins involved in LOS transport to the outer membrane caused drug hypersensitivity in at least two of the three pump overproducers. On the other hand, depletions of translation-associated proteins, as well as components of the proton-pumping ATP synthase pump resulted in fitness benefits for at least two pump-overproducing strains in the presence of the drug. Therefore, pump overproduction exacerbated stress caused by defective outer membrane integrity, while the efficacy of drug resistance in efflux overproducers was enhanced by slowed translation or defects in ATP synthesis linked to the control of proton movement across the bacterial membrane.

53 **Introduction**

54 *Acinetobacter baumannii* is a Gram-negative nosocomial pathogen that presents as
55 ventilator-associated pneumonia, bacteremia, and urinary tract infections (1-3). The difficulty in
56 combating diseases caused by this organism, often associated with multidrug-resistant (MDR)
57 isolates, has stimulated a demand for new antimicrobials or improved therapeutic strategies that
58 can overcome the high rates of MDR among clinical isolates, making this organism a high
59 priority for developing new therapeutic strategies (1, 3). Among the various determinants of
60 resistance to currently available drugs, hyperexpression of drug efflux pumps is the one
61 mechanism that is commonly associated with MDR across multiple species (4-9). The resistance-
62 nodulation-division (RND) pump class provides the most clinically relevant strategy for
63 extruding antibiotics in *A. baumannii,* with the AdeABC, AdeIJK, and AdeFGH efflux pumps
64 being the most frequently associated with MDR (6-9). Therefore, strategies that target isolates
65 overexpressing these pumps or which hypersensitize these strains to antibiotics are of great
66 interest.

67 For Gram-negative organisms, the primary route to fluoroquinolone resistance is
68 acquisition of target site mutations in the active sites of the major type II topoisomerases in the
69 cell, DNA gyrase and topoisomerase IV (10). In most *A. baumanni* clinical strains that have been
70 sequenced, mutations in both *gyrA* and *parC* are found, encoding the A subunits of gyrase and
71 topo IV respectively (10). Based on MIC testing and sequencing of isolates, clinical strains also
72 commonly have a third mutation in one of the regulatory genes that activate an RND antibiotic
73 efflux pump. Mutations in these genes, encoded by *adeS*, *adeN*, or *adeL*, upregulate the
74 AdeABC, AdeIJK, or AdeFGH efflux pumps respectively, and result in high fluoroquinolone
75 resistance (FQR) (7, 11-15).

76 Previous work identified mutations that caused strain-specfic vulnerabilities of pump
77 overproduction in nonessential *A. baumannii* genes. These mutations caused retarded growth of
78 strains overproducing efflux pumps, or synergized with the fluoroquinolone ciprofloxacin to
79 hypersensitize the overproducers to the drug (16). Based on this work, lesions in nonessential
80 genes that are predicted to alter outer membrane integrity sensitize efflux pump overproducing
81 strains to ciprofloxacin treatment. Furthermore, strains having activating mutations in *adeL*
82 (AdeFGH overproduction) appeared to induce a stress response in the absence of antibiotics that
83 mimics what is observed in the presence of ciprofloxacin and other antibiotics (17). This may be
84 due to a special feature of the pump or because of extreme overexpression of the *adeFGH* locus
85 relative to other pump-overexpressing strains (16).

86 Most effective antimicrobial targets are in proteins that are essential for growth.
87 Therefore, when identifying mutations preferentially sensitizing strains that overproduce efflux
88 pumps, it is desirable to identify mutations in essential genes. To approach this problem, we usde
89 a CRISPRi approach in this work to target essential genes with sgRNAs. The library design took
90 advantage of a previously developed strategy that allowed the generation of multiple
91 hypomorphic alleles with varying fitness defects in each essential gene, to allow the discovery of
92 depletions that show strain-specific aggravation of drug sensitivity (18-20). Depletions that
93 cause drug hypersensitivity were found to predominantly target proteins involved in maintaining
94 outer membrane integrity, with most of these targets responsible for LOS biogenesis and
95 transport. Interestingly, interference with translation and the assembly of the proton pumping
96 F1F0 ATPase provided the FQR strains with a fitness advantage in the presence of drug, pointing
97 to targets that collaborate with efflux pump overexpression to promote drug tolerance. A recent

98 study has also used CRISPRi to identify candidates that have altered sensitivities to rifamycin
99 and polymyxins in *A. baumannii* (21).

100

101 **Results**

102 **Development of a CRISPRi strategy to uncover hypomorphs with reduced fitness in**
103 **FQR strains.** In our previous study (16), we identified transposon insertion mutations that
104 reduce the fitness of efflux pump overproducers or that specifically hypersensitize these variants
105 to ciprofloxacin. Except for very rare exceptions (22), insertion mutations could only be
106 analyzed in nonessential genes. This interfered with our ability to identify proteins encoded by
107 the essential gene set that could similarly sensitize pump overproducers. To overcome this
108 shortcoming, we devised a CRISPRi screening strategy to identify depletion variants with
109 decreased fitness in the presence of drug or showed fitness defects in a subset of strains, but still
110 allowed viability of the bacterium as previously described (Fig. 1) (18, 23). Using a pool design
111 similar to that used for eukaryotic cells (18, 23), and sequencing data of a previously generated
112 dense transposon bank in the ATCC 17978UN strain background (16, 22, 24), the insertion
113 landscape was inspected to identify essential genes, based on open reading frames (ORFs)
114 having significantly reduced or no insertions (Materials and Methods (25, 26)). After comparison
115 to similar insertion mutation studies in *A. baumannii*, a strain list of 406 essential genes was
116 generated (24, 27, 28).

117 A single 24-nucleotide sgRNA was designed for each essential gene by identifying the
118 PAM site on the noncoding strand most proximal to the translational start. For each perfect
119 sgRNA, we also devised a set of 23 mismatch sgRNAs that differed from the original guide

120 sequence by 1 or 2 nucleotides at varying locations across the sequence, as previously generated
121 for mammalian systems (18). We also created 5 shuffle sgRNAs comprising the same
122 nucleotides in a disordered fashion to use as negative controls, anticipating that they would have
123 a neutral effect on fitness. An additional collection of approximately 200 shuffle sgRNAs were
124 created with minimal anticipated homology to the genome as well, called pool shuffles. The final
125 library consisted of approximately 12,000 sgRNAs that had a size and complexity similar to a
126 previously constructed model pool (Fig. 1) (18). To facilitate cloning, the pWH1266 shuttle
127 vector was converted into a GoldenGate-compatible plasmid to allow efficient construction of
128 the sgRNA library via insertion of the duplex target oligonucleotides from the pool into the site
129 generated by a Type II restriction enzyme (see Materials and Methods). This facilitated easy
130 reconstruction of individual clones for further analysis. Control of CRISPRi-dCas9 targeted
131 depletions was provided by a tetracycline inducible dCas9 introduced into the genomes of the
132 WT and FQR pump overexpressing strains as described previously ((24); Materials and
133 Methods). These strains were then transformed with the CRISPRi sgRNA-pDNA bank, ensuring
134 at least 10^6 colonies were pooled.

135 **Strategy for identifying sgRNAs that result in a gradient of fitness defects.** To
136 demonstrate that the CRISPRi-dCas9 strategy allows us to perform stoichiometric depletion of
137 essential genes based on using mismatched sgRNAs, the pool harbored in WT ATCC 17978UN
138 was grown in LB broth in the presence of anhydrotetracycline (aTc) to induce dCas9 expression
139 for 7-8 generations based on A_{600} measurements (Materials and Methods). This growth strategy
140 was chosen so that we could determine fitness values for each individual guide using the same
141 quantitative fitness measurements used for Tn-seq (Materials and Methods; (10, 22). Of note,
142 there was no discernable growth deficit of the overall pool after 7-8 generations of growth in the

143 presence of the aTc inducer when compared to growth in its absence in the WT *A. baumannii*
144 strain. Therefore, cultures were harvested either prior to addition of aTc (timepoint T1) or
145 following bank outgrowth for 7-8 generations after induction of dCas9 (timepoint T2). Plasmid
146 DNA harboring the sgRNA coding sequences was then extracted at both timepoints, the sgRNA
147 region was amplified from the extracted plasmid DNA, barcoded, and prepared for sequencing to
148 calculate fitness of each derivative (Materials and Methods; Fig. 1). Reads were then processed
149 and assigned to their respective guide in the sgRNA library to determine the abundance of each
150 unique sgRNA in all conditions. The data were used calculate the fitness of each derivative, and
151 displayed as statistical significance as a function of fitness compared to absence of induction
152 (Materials and Methods).

153 Investigating the read distribution for the sgRNAs in the sgRNA-pDNA library, we
154 observed a normal distribution of reads assigned (Supp. Fig. 1A). After introduction into the WT
155 *A. baumannii* strain, this distribution was maintained (Supp. Fig. 1B), and a similar distribution
156 was maintained in the shuffle sgRNAs after induction (Supp. Fig. 1C), consistent with
157 nontargeting behavior as expected for negative/neutral controls. We conclude that the bank can
158 be transferred and maintained in *A. baumannii* to allow analysis of CRISPRi-dCas9 depletions
159 for the purpose of constructing hypomorphic alleles in essential genes in multiple strain
160 backgrounds.

161 **Strains show low fitness when harboring sgRNAs with perfect sequence identities to**
162 **essential genes.** Fitness was calculated after stoichiometric depletion of target genes across
163 replicate cultures and fitness scores resulting from sgRNA depletion were calculated as
164 previously described for 7-8 generations of growth of Tn-seq pools (Materials and Methods (22,
165 29)). Fitness values were subsequently normalized to 23 shuffle sgRNAs that had no statistically

166 significant effect on fitness relative to the entire pool. The fitness values for this subset of shuffle
167 sgRNAs remained neutral despite the induction of dCas9 (Fig. 2A, yellow circles). On the other
168 hand, most sgRNAs with perfect homology to their essential gene targets diminished fitness
169 upon dCas9 induction (Fig. 2B). Although only a single 24 base region of each essential gene
170 was chosen for targeted knockdowns, the majority of perfect match oligonucleotides
171 (approximately 62% per Fig. 2D) showed fitness defects where the fitness difference due to
172 induction was less or equal to -0.1 after 7-8 generations of growth.

173 **The sgRNAs with mismatched bases proximal to the PAM site showed improved**
174 **fitness relative to guides with perfect sequence identity.** It has been demonstrated that
175 nucleotide mismatches closest to the 3' PAM site that are critical for dCas9 targeting were found
176 to reduce knockdown efficiency (18, 19). We observed this trend for fitness calculations as well
177 (Fig. 2B as compared to Fig. 2C), as 33% of the -1 or -2 mismatches had fitness defects ≤-0.1
178 relative to the mean (defects between -0.1 and -0.5), while for the perfect guides, 70% were in
179 this range while also passing the false discovery rate (FDR: q value ≤0.05 (Fig. 2D)). This
180 pattern can be seen more clearly by focusing on individual genes. In the case of *gyrA*, encoding
181 subunit A of DNA gyrase, the perfect guide sgRNA had a fitness of 0.44 if normalized to the
182 fitness score in the absence of induction (Fig. 2E, F respectively). On the other hand, mismatches
183 at -1 or -2 had mean fitnesses of 0.73-0.95, normalized to the fitness score in uninduced culture
184 (Fig. 2E, F respectively). We also found that guides with double mismatches close to the PAM
185 site resulted in particularly mild effects on fitness, with many of these being indistinguishable
186 from the shuffle guides (Fig. 2F).

187 **Flexibility in choice of sgRNA sequence location with respect to translation start**
188 **codon.** 25% of the perfect guides that generated fitness score differences >-0.1 (between 90-

189 100% the fitness of the mean; Fig. 2D) may have had mild impacts as a result of a variety of
190 factors, one of which may be attributed to the relative distance of the target sequence to its
191 translation start codon, but such a relationship was difficult to establish (Fig. 3A-D). For
192 instance, about 4.2% of the exact match guide sequences that were located 25-30 nucleotides
193 away from the start codon yielded fitness defects ranging between -0.5 to -0.4, while those with
194 fitness defects of 0.0 to -0.1showed a similar frequency (green bars; Fig. 3D). On the other hand,
195 about 13% and 16% of guides located 1-6 nucleotides away from the start codon yielded fitness
196 defects between -0.5 and -0.4 or -0.1 to 0 respectively (dark grey bars; Fig. 3D). This is
197 consistent with a slight skewing toward higher efficiency for targets closer to the translation start
198 site, but the fraction of guides located distant from the start site was too small to analyze
199 statistically. To determine if poor target depletion was responsible for the mild fitness effects
200 witnessed by these guides, transcript levels of four targets were determined by q-rtPCR alongside
201 an effective *gyrA* guide. The *gyrA* guide showed 96% depletion relative to the absence of aTc
202 addition, while the small fitness defect strains varied from 32%-90% depletion relative to that
203 seen in the absence of induction (Supp. Fig. 2). This is consistent with weak fitness defects being
204 caused by inefficient depletion.

205 **Extended outgrowth of the sgRNA bank amplifies subsequent changes in fitness.** As
206 70% of the perfect sgRNAs generated significant fitness effects and resulted in fitness values ≤-
207 0.1 relative to uninduced levels after 7-8 generations with inducer, fitness defects may be more
208 pronounced by allowing the bank to grow further than 8 generations. To test this hypothesis, five
209 replicate cultures of both the WT and *gyrAparCadeS* (GPS) strains were grown for 14-16
210 generations by diluting the cultures after 7-8 generations into fresh media and incubating a
211 further 7-8 generations in the absence and presence of aTc inducer. The fitness scores yielded by

212 each sgRNA after 14-16 generations were compared to those observed in 5 replicate cultures for
213 strains grown for 7-8 generations. Fitness of the depletion strains was then calculated identically
214 under both culture conditions, incorporating the different expansion factors from both outgrowth
215 experiments (Supp. Data 3).

216 It was evident that the longer culture period amplified the fitness changes observed, and
217 that the number of perfect guides that failed to show significant fitness defects was reduced to
218 just a few, particularly in the GPS background (Fig. 4F). This was consistent with the target
219 proteins being subjected to turnover and possibly dilution through bacterial division. Almost the
220 entire bank of hypomorphs showed lower fitness scores after 14-16 generations of induction
221 compared to 7-8 generations in both WT (Fig. 4A) and in GPS strains (Fig. 4B). Noteworthy is
222 the shift in fitness of the perfect guides after a longer incubation, as the population of perfect
223 guides which showed weak defects after 7-8 generations (Fig. 4C, E, black circles) joined a
224 tighter distribution of guides that had strong effects (Fig. 4D, F, black circles). After 7-8
225 generations of induction of the WT sgRNA bank, about 5% of perfect sgRNAs caused fitness
226 defects by at least -0.5, whereas approximately 40% reached this level after 14-16 generations
227 (Fig. 4C vs Fig. 4D). Similar results were found in the GPS strain background (Fig. 4E, F).
228 These data indicate that the defects observed in hypomorphs can be aggravated by challenging
229 the sgRNA banks for longer periods of time.

230 The fitness differences yielded by the shuffle guides did not shift substantially between
231 culturing for 7-8 versus 14-16 generations. While 0.09% of shuffles caused fitness differences
232 equal to or less than -0.5 after culturing the WT bank for 7-8 generations, only 0.76% do after
233 14-16 generations (Supp. Fig. 3A, B). This was similarly observed with the GPS bank (Supp.

234 Fig. 3C, D). These changes were minor compared to those witnessed by the perfect guides, as
235 would be expected of guides that have neutral effects on bacterial fitness.

236 **Identification of hypomorphs with altered fitness in the FQR strain backgrounds**.
237 From our initial screen (Fig. 2), fitness values derived from each sgRNA were compared
238 between the FQR (GPS) and WT drug-susceptible strains via multiple t-test analyses, comparing
239 each unique sgRNA individually rather than pooling all the data for each gene (Materials and
240 Methods). The difference in fitness generated by each sgRNA between the two strains was
241 calculated, and fitness scores were determined as described (Materials and Methods). No
242 candidates were identified using the mean of three cultures, indicating that candidate
243 identification required increasing the number of replicates analyzed, increasing the number of
244 generations, and/or the addition of drug stress. Growing additional cultures in parallel (n=10)
245 identified a number of targets that significantly influence the fitness of GPS compared to WT in
246 the absence of any drug pressure (Supp. Fig. 4A,B). Focusing on sgRNAs yielding fitness score
247 differences by at least 20% revealed that multiple different sgRNA depletions of anti-transcription
248 termination factor *nusG* showed profound reductions in GPS fitness when compared to WT
249 (Supp. Fig. 4A). Expanding the criteria for fitness differences to a minimum of 10% unveiled an
250 additional 27 targets that reduced GPS fitness relative to WT, including proteins involving
251 secretion across the inner membrane (*secY, secA, ffh)* as well as DNA replication, the electron
252 transport chain, and the TCA cycle (Supp. Fig. 4B). Comparing the fitness of the hypomorphs
253 after 14-16 generations of growth in the absence of drug between GPS and WT (n=5) also
254 uncovered a number of additional targets that showed strain-dependent fitness effects. Notably,
255 depletion of factors involved in competing processes resulted in opposite phenotypes. For
256 example, depletion of the transcription termination factor Rho improved fitness of the GPS

257 mutant relative to WT, while depletions of the anti-terminator NusG showed stronger fitness
258 defects in the GPS strain when compared to WT (*nusG* and *rho*; Supp. Fig. 4A, 4C, 4D).

259 **Identification of targets that significantly alter the fitness of high-level FQR strains.**
260 We next introduced the sgRNA pool into a panel of strains having the *gyrAparC* background
261 with either the *adeS*, *adeN,* or *adeL* pump overproducing mutations (GPS, GPN, and GPL
262 respectively), using increased numbers of replicates (Materials and Methods). The libraries in
263 four strains (WT, GPS, GPN, and GPL backgrounds) were grown in rich broth in the presence or
264 absence of the aTc inducer (for dCas9 expression) and in the absence or presence of sub-MIC
265 levels of ciprofloxacin using concentrations that resulted in 20-30% growth inhibition across the
266 strains. The statistical significance of each depletion was calculated as a function of the change
267 in fitness, determined by multiple t-test comparisons using an FDR of q value<5% (Supp. Data 4;
268 Materials and Methods)(30). Discoveries showing a significant fitness shift between each
269 comparison were sorted to identify sgRNAs yielding fitness difference scores ≥ 0.2 (knockdown
270 imparting a fitness benefit or alleviated effect) or ≤ -0.2 (knockdown causing a fitness defect or
271 aggravated effect) relative to WT. Among these, targets that were represented by 3 or more
272 guides from their sgRNA set were identified as top discoveries.

273 **Identifying targets that are shared between multiple FQR strains.** We next identified
274 the top discoveries (FDR<5%; fitness difference≤-0.2 or ≥0.2), revealed by comparing the FQR
275 strains to WT in absence (Untx FQR-WT) or presence (Ciptx FQR-WT) of drug treatment. In
276 addition, the top discoveries were identified by fulfilling the same criteria (FDR<5%; fitness
277 difference≤-0.2 or ≥0.2) in the presence vs absence of drug for each FQR strain (Ciptx-Untx)
278 (Figs. 5,6). Analysis of the data in the presence and absence of ciprofloxacin gave three notable
279 outcomes. First, in the absence of antibiotic, there were very few candidates that pass the

280 statistical bar set in these studies, further supporting the Tn-seq results indicating that *A.*
281 *baumannii* is quite tolerant of pump overproduction (16). This was particularly true of the GPS
282 strain, indicating that overproduction of the AdeAB pump is well tolerated by *A. baumannii* (Fig.
283 6B). This may be connected to the fact that, unlike the other FQR strains, the GPS mutant does
284 not overexpress the outer membrane component of the efflux system (11). Secondly,
285 knockdowns in *nusG* resulted in lowered fitness of all three drug efflux pump overproducers in
286 the absence of drug. The NusG protein supports transcription elongation in *E.coli* (31), most
287 thoroughly analyzed in the context of the ribosomal RNA operons (32). Thirdly, unique among
288 the three FQR strains, depletion of cell wall factors specifically resulted in fitness defects in the
289 *adeL* pump-overproducing mutant (Fig. 5). This supports the previous Tn-seq data in which loss
290 of cell envelope components selectively hypersensitized the GPL strain compared to the other
291 pump overproducers (16).

292 Heatmap analysis indicated that there were several targeted depletions that have similar
293 phenotypes in more than one pump overproducer (Fig. 5). Therefore, the entire dataset was
294 analyzed in the presence or absence of drug, and targets were identified that were shared by two
295 or more strains or which were unique to a single pump overproducer (Fig. 6, Supp. Data 4). This
296 analysis revealed that the presence of drug identified a number of loci that caused increased
297 sensitivity to drug relative to WT. Furthermore, it identified a number of essential genes whose
298 activities interfered with the fitness of FQR strains in the presence of drug.

299 **Disruption of either ribosome biogenesis or F1F0 ATPase assembly shows inverted**
300 **consequences relative to depleted LOS biosynthesis.** The analysis of the entire dataset of
301 fitness challenges for GPS (Fig. 7A), GPN (Fig. 7B), and GPL (Fig. 7C) compared to WT in the
302 presence or absence of ciprofloxacin, revealed a number of clear patterns. Consistent with all

303 analyses of fitness in the presence of ciprofloxacin, the GPL strain yielded the most depletions
304 that resulted in altered fitness (Figs. 5A), with only a few targets identified in the GPS
305 background (Fig. 5C). Depletion of *lpxC* and *lpxD* genes, encoding LOS biogenesis proteins,
306 uniformly caused fitness defects relative to WT in the presence of drug, even for the robust *adeS*
307 mutant (Fig. 7A, Supp. Fig 3). With GPN and GPL, the spectrum of depletions that caused
308 fitness defects was expanded to include a number of other loci involved in LOS biosynthesis
309 (*kdtA*, *kdsD*) (Figs. 7B, C, Supp. Fig. 5), as well as a large cluster of genes involved in LOS
310 transport to the surface (*lptA-D*, *lptG*) (Figs. 7B, C, Supp. Fig. 5). These data emphasize that
311 outer membrane integrity maintenance is required for FQR survival in the presence of drug, with
312 factors controlling the composition of LOS being particularly important. Of note is the fact that
313 depletions of BamD had weaker effects on the GPS overproducer than the other two FQR strains,
314 consistent with our observation that there were fewer hypomorphs interfering with composition
315 of the outer membrane that reduced GPS fitness (Fig. 6,7). Notably, activation of the *adeS*-
316 regulated system does not result in overexpression of its outer membrane protein component,
317 which would likely be linked to hypersensitizing defects in outer membrane biogenesis.

318 Our most surprising result is that depletion of a number of loci associated with translation
319 very strongly increased fitness of all three FQR strains relative to WT. Most of these loci are
320 involved in ribosome assembly or modification enzymes (*obgE, rimM*), consistent with slowing
321 translation and accumulating alarmones associated with translational stalling. Supporting this
322 hypothesis is the fact that in the GPL strain, depletion of *spoT,* predicted to prevent degradation
323 of ppGpp-associated alarmones and result in their accumulation, similarly increased fitness of
324 this pump overproducer (Fig. 5A). There was also a clear demonstration of increased fitness
325 exhibited by depletions of the F_1F_0 proton-pumping ATPase/synthase in the presence of

326 ciprofloxacin, tying fitness to the overall proton gradient of the cell. Unlike *E. coli* (33), the ATP
327 proton pump is an essential protein for *A. baumannii* growing in rich culture medium, consistent
328 with it playing an important role in maintaining membrane potential. As the function of the
329 antibiotic efflux pumps is to antiport drugs in exchange for protons, decreased F_1F_0 ATP
330 synthase activity may remove an important competitor for protons or facilitate cytoplasmic pH
331 homeostasis.

332

333 **Discussion**

334 Understanding how *A. baumannii* MDR strains tolerate pump overproduction and what
335 proteins support pump hyperactivity is of great importance, because MDR is often driven by
336 hyperexpression of RND drug efflux pumps that can export a broad array of substrates. In this
337 work we devised a CRISPRi screen to find essential gene candidates that support the fitness of
338 FQR pump overproducing strains. This approach showed that depletions of genes that encode
339 LOS synthesis (multiple *lpx* loci, *kdtA*/*waaA*, and *kdsD*/*kpsF*), LOS transport proteins (multiple
340 *lpt* loci), as well as encoding a component required for proper outer membrane protein
341 localization (*bamD*) reduce fitness of pump overproducers in the presence of antibiotic
342 treatment.

343 BamD, which is important for FQR fitness in the presence of ciprofloxacin, is essential
344 for the assembly and proper insertion of outer membrane proteins (OMPs) (34). Interestingly, we
345 previously showed that transposon knockouts of SurA, a nonessential periplasmic chaperone
346 with similar function to BamD, reduces GPL strain fitness in the presence of Cip (16,34).
347 Depletion of BamD may interfere with the proper assembly of the pump outer membrane factor

348 and other OMPs that maintain the outer membrane barrier (35). Alternatively, the fact that
349 components of the complex involved in the presentation of unfolded precursors to BamA lower
350 fitness in the presence of drug is consistent with an unloaded Bam complex being specifically
351 toxic to the cell envelope. Perhaps a Bam complex unable to load precursors increases outer
352 membrane permeability, overwhelming the ability of the pump to efflux drug.

353 Targets involved in the synthesis and transport of LOS are likely candidates for
354 sensitization of pump-hyperexpressers for reasons similar to the Bam complex, as they
355 contribute to the stability of the transporter and membrane integrity. The Lpt proteins are part of
356 a large system that is essential to the transport of LOS to the outer membrane. Decreased levels
357 of these proteins compromise the membrane barrier and produce a defective cell envelope that
358 results in accumulation of material in the periplasmic space (36, 37). Mutations in *lpxC* and
359 *lpxD,* whose products act early in the LOS synthesis pathway just after LpxA, result in LOS
360 deficient cells (38, 39). *Acinetobacter baumannii* is one of three species that can survive without
361 LOS at a great fitness cost (38, 39), although the strains used in our study are derived from *A.*
362 *baumanni* ATCC 17978, which is likely inviable in the absence of LOS (40). Null mutations in
363 genes *pbpG* and *lpsB* reduce overall LOS levels and alter LOS composition respectively (16, 22),
364 and we previously identified each as fitness determinants of the FQR strains based on transposon
365 mutagenesis (16). Targeting these proteins that control LOS dynamics may diminish the integrity
366 of the outer membrane and facilitate drug entry, but this does not explain why fitness is more
367 severely compromised in the high-level FQR pump hyper-expressers than in the WT or in the GP
368 strains. One explanation is that there is direct binding of LOS to the RND transporter complex,
369 and the absence of this lipid results in destabilization of the outer membrane component of the
370 transporter. It is known that LPS can bind OMPs and that interfacing lipids may mediate OMP

371 self-association, likely contributing to outer membrane integrity (41, 42). Overall, the targets
372 revealed by this work indicate that the FQR pump hyperexpressors are more vulnerable to
373 changes in the outer membrane composition than strains lacking these pumps. Components that
374 support maintaining the integrity of the permeability barrier as well as stabilize the RND drug
375 transporters are likely to be important for survival during drug treatment.

376 Also notable in our work were hypomorphs that conferred a fitness advantage for strains
377 hyperexpressing efflux pumps in the presence of Cip, such as depletion of genes that direct the
378 assembly of the inner membrane-associated F_1F_0 ATPase/synthase (*atpI* and *atpF* in multiple
379 FQR strains, as well as five other *atp* genes in GPL) and translation (*fmt*, *rimM*, *der/engA*, *rnpA*).
380 The F_1F_0 ATPase/synthase complex is known to both synthesize and hydrolyze ATP, using
381 proton motive force (PMF) to pump protons in and generate ATP or reversibly hydrolyze ATP to
382 pump protons out of the cytosol (43-45). AtpF encodes the ATPase B subunit that links the F_1
383 catalytic domain to the F_0 membrane spanning proton translocator, which links ATP generation
384 and hydrolysis to proton pumping by F_1 (45-47). AtpI on the other hand functions as a
385 chaperone, a non-structural component that is poorly conserved, which promotes the formation
386 of the F_0 c-ring as well as the stability of the complex (48, 49). Perhaps targeting these
387 components is sufficient for the changes in fitness that we observe while limiting the lethality
388 resulting from inhibition of the complex. Overall, the F_1F_0 ATPase/synthase complex could play
389 a compensatory role for high pump activity during which proton influx accompanies substrate
390 egress, as the ATPase extrudes protons back out of the cell to establish PMF and alleviate
391 cytosolic acidification. This is consistent with our previous observation that there were
392 significantly reduced numbers of viable transposon insertion disruptions in the cytochrome b_o (3)
393 ubiquinol oxidase complex in the GPL strain, which similarly extrudes protons (16). Given the

394 importance of the ubiquinol oxidase complex, it is also possible that the ATPase/synthase acts as
395 a competitor for protons during ATP synthesis which are extruded by the RND drug egress
396 system. Removal of the competitor allows a source of protons for the drug antiporters.

397 There may be an explanation for the fitness advantage of ATP synthase depletion that is
398 consistent with the idea that increased fitness in the presence of the drug is associated with a
399 dormancy-like state. Perhaps allowing the GPL mutant to enter an ATP-depleted dormant state
400 allows it to transiently cope with both pump overproduction and drug stress. Interestingly, in our
401 RNA-seq experiments, we found that *atpE* transcription was significantly downregulated in the
402 GPL mutant when compared to the GP strain grown in the absence of drug (16). Although
403 depletion of this critical F_0 component was not shown to protect from drug action, it does
404 emphasize the similarity between drug stress and stress related to overproduction of the AdeFGH
405 pump. The abundance of fitness determinants and genes that are differentially regulated in the
406 GPL mutant portrays the consequence of pump overproduction in the presence and absence of
407 drug pressure. It also indicates that manipulation of the proton motive force may be a critical
408 determinant in protecting against both protein overproduction and antibiotic stresses.

409 Depletions that are predicted to reduce translation efficiency similarly promote fitness in
410 the pump overproducers in the presence of the drug. Both lowered ATP and reduced translation
411 have been associated with persister cell formation, allowing bacteria to better cope with the
412 stress they are experiencing during drug treatment and to survive drug activity that targets active
413 processes (50, 51). Pump hyperexpression has been documented to contribute to the development
414 of persistence (52), and hyperexpression of the AdeFGH efflux pump similarly promotes
415 persistence (53). Therefore, both reduced ATP synthesis and translation could be advantageous
416 for pump hyperexpressors, allowing survival in the presence of high levels of drug combined

417 with the stress imparted by elevated levels of transporter. Our data indicate that using drugs that
418 impede translation may antagonize ciprofloxacin treatment. Future efforts will be directed to
419 exploring these hypotheses in hopes of better understanding the limitations of pump over-
420 expression and identifying proteins that help support the viability of the MDR state.

421

422 **Acknowledgements**

423 This work is supported by NIAID grants U01AI124302, R21AI128328, and U19AI142780. We
424 thank Defne Surujon (Boston College) for the sam-to-wig file conversion script, Yunfei Dai
425 (Northeastern University) for communications regarding dCas9 strain generation, sgRNA design,
426 and TRANSIT, and for the pUC-Tn7-GentR-pTet::dCas9 and pWH1266-sgRNA plasmids,
427 Rebecca Batorsky at Tufts Technology Services for aiding with TRANSIT accessibility, and
428 Albert Tai at Tufts Genomics Core Facility for communications regarding sequencing and library
429 preparation.

430

431 **Materials and Methods**

432 **Bacterial strains and growth conditions**. Bacterial strains used in this work are listed in
433 Supplementary Data 1. All *Acinetobacter baumannii* strains are derived from ATCC 17978UN.
434 Cultures were grown in lysogeny broth (LB) (10 g/L tryptone, 5 g/L yeast extract, 10 g/L NaCl)
435 or on LB agar plates (LB supplemented with 15g/L agarose). For growth in broth culture,
436 bacteria were aerated at 37°C on a platform shaker or a roller drum, with growth monitored by
437 measuring absorbance via a spectrophotometer at 600 nm (A_{600}). Superoptimal broth with
438 catabolite repression (SOC) was used for recovery following all electroporations of *A.*

439 *baumannii.* Electroporations were performed using 0.1cm gap cuvettes and Bio Rad Gene Pulser,
440 with the settings 200 Ω, 25 µF, and 1.8 kV. LB was supplemented with antibiotics, as needed, at
441 the following concentrations: Carbenicillin (Carb): 50/100µg/mL, Gentamicin (Gent): 10µg/mL,
442 or Chloramphenicol (Cm): 10/25µg/mL.

443 **Molecular cloning and mutant construction.** Primers (IDT) and plasmids used
444 throughout this study are listed in Supplementary Data 1. The dCas9 construction is tetracycline
445 (Tet)-inducible and chromosomally embedded at the Tn7 site in the four strains of interest. The
446 plasmids and techniques used to create these strains are as previously described (23, 24). Briefly,
447 the mobile Tet-inducible dCas9 was introduced into the four *A. baumannii* recipient strains of
448 interest via four parental mating and Tn7 transposition. The recipient *A. baumannii* strains, the
449 HB101 RK600Cm^{R} helper, DH5a λpir (pTNS3) encoding the T7 transposase, and the DH5a
450 (pUC-Tn7-GentR-pTet::dCas9) donor strain were grown overnight in LB broth with appropriate
451 antibiotics. The following day the cultures were normalized to A_{600} of 2.0 and 100µl of each of
452 the three *E. coli* cultures were combined with 100µl of each *A. baumannii* recipient culture in
453 600µl LB broth, prewarmed to 37ºC. The mixture was washed twice in 37ºC LB broth, then
454 resuspended in 25µl of fresh broth and spotted on pre-warmed LB agar plates. These plates were
455 incubated at 37ºC for approximately 5 hours then resuspended in 1mL sterile phosphate buffered
456 saline (PBS) before plating and overnight selection on Vogel-Bonner minimal medium (VBM)
457 containing 10µg/mL of Gent to select against E. coli strains and the parental Gm^{S} *A. baumannii*.
458 Exconjugants were colony-purified on VBM containing10µg/mL Gm, and screened on LB agar
459 with 100µg/mL Carb and on LB agar with 10µg/mL Gm. The insertion at the *att*Tn7 site
460 downstream the *glmS* gene was confirmed by colony PCR using the primers glmS2-F1 and
461 Tn7R-R1.

462 The vector pWH1266 used to introduce the sgRNAs is a shuttle plasmid previously
463 described (24) containing origins of replication of pBR322 and an origin of replication from a
464 natural *Acinetobacter* isolate (24) to allow for propagation in both *E. coli* and *A. baumannii*
465 respectively. It encodes for the β-lactamase gene (*bla*) on the backbone and contains a sequence
466 to be replaced by the sgRNA sequences upstream of the dCas9 handle and *S. pyogenes*
467 transcriptional terminator, with the fusion driven by the constitutive synthetic promoter pJ23119.
468 For efficient cloning of sgRNAs, the vector was made GoldenGate™-compatible by first
469 removing the single BsaI Type II restriction site present in the *bla* gene and then introducing two
470 BsaI sites between the promoter and dCas9 handle to allow for directional sgRNA oligo
471 insertion. Using this backbone, all 24nt sgRNA oligos were constructed with additional 4nt
472 overhangs that allowed for directional cloning. The sgRNA bank was designed by loosely
473 following a previous strategy for stoichiometric knockdowns (18), and the vector and library
474 design were used for construction of the sgRNA-plasmid library by contract (GeneWiz).

475 **Identification of essential genes in *Acinetobacter baumannii*.** Essential genes of *A.*
476 *baumannii* ATCC 17978UN were determined using transposon mutagenesis sequence data in the
477 WT strain (16, 22), and the data from that study was subjected to TRANSIT Gumbel analysis to
478 identify the essential genes (24-26). Briefly, sequence mapped SAM files were converted to wig
479 files with a custom python script bowtie_to_wig2.py provided by Defne Surujon from the Tim
480 van Opijnen lab. The wig files were then used as input, using the TRANSIT Gumbel analysis
481 pipeline (26) with default settings. Cross referencing our list of essential genes to those similarly
482 identified in other studies in the same strain or the more recently isolated AB5075 clinical strain
483 revealed 406 genes exhibiting a high likelihood of essentiality, given their classification as
484 essential in at least one of the other published analyses as well (24, 27, 28).

485 **sgRNA library design**. The 24nt sgRNAs were principally designed (to target each
486 essential gene) with the antisense strand sequence using a PAM site on the antisense strand that
487 is as close as possible to the translational start site. The sgRNA pool was then expanded with an
488 additional 23 mismatch sgRNAs that differ from each targeting sgRNA by 1 or 2 nucleotides,
489 along with 5 shuffle sgRNAs that comprise the same nucleotides as the original target-
490 homologous sgRNA but are shuffled to minimize the likelihood of off-target effects. An
491 additional 216 "pool shuffle" sgRNAs of an array of nucleotides with the GC content of the
492 targeted genes designed to minimize homology to any genomic sequence, bringing the final
493 sgRNA pool to 12,000 sgRNAs total (Supp. Data 2). Mismatches were employed to introduce
494 sgRNAs with reduced knockdown efficiencies, while the shuffles served as negative controls
495 (anticipated to provide a neutral effect on fitness). A BLAST search did reveal that up to 12bp
496 overlap with the genome was unavoidable among some members of the control pool. These
497 mismatches and shuffle sgRNAs were designed as previously described (18), using the python
498 script 'final sgRNA dirty pool design.ipynb' (GitHub).

499 **Preparation of pools with sgRNA library.** The sgRNA-pDNA library was introduced
500 into the FQR pump hyper-expressors and WT strain with chromosomally encoded Tet-inducible
501 dCas9 via electroporation. About 50ul electrocompetent cells were transformed with 23-46ng of
502 the pDNA, the resuspended mixture diluted 1/10, and 200µl plated on five large pre-warmed
503 SOC agar plates overlain with mixed cellulose ester filters (0.45µm pore size, 137mm diameter,
504 Advantec). The mixture was spread on the filters using beads. This was repeated for a total of 3
505 transformations per strain background. These transformants were allowed to recover at 37°C for
506 an hour on SOC agar plates before the filters were transferred to selective LB agar plates
507 containing 50µg/mL Carb and incubated overnight at 37°C for about 13.5-14 hours. The

508 following day, filters were pooled to acquire somewhere around 250,000-350,000 CFUs,
509 estimated based on using image analysis of previous pools (ImageJ). Pooling entailed washing
510 colonies off with 100mL sterile PBS with gentle shaking in a sterile round bottom 3L beaker.
511 Glycerol was added to a final concentration of 10-20% and 1mL aliquots were placed into
512 cryotubes for -80°C storage until needed.

513 **Identification of hypomorphs with fitness defects**. Following previous protocols for
514 determining fitness using Tn-Seq pools (10, 22), each vial of *A. baumannii* P_{Tet}::dCas9 harboring
515 the sgRNA array was thawed on ice, diluted into 25mL LB broth to an A_{600}=0.1, and revived by
516 incubation at 37°C with shaking for 50min-60min until they reached around A_{600}=0.2. Each
517 culture was then diluted to an A_{600}=0.003 in 10mL LB broth in the absence or presence of either
518 50ng/mL, 100ng/mL, or 200ng/mL aTc for dCas9 induction and the fluoroquinolone
519 ciprofloxacin. Cultures were incubated for approximately 7-8 generations on the drum wheel at
520 37°C until densities reached A_{600}= 0.635-0.895 (average 0.75). The cultures were harvested both
521 before (T1) and after (T2) dCas9 induction and drug treatment to allow sgRNA fitness analyses.
522 Sample pellets were stored at -20°C until all were collected. Plasmid was extracted from each
523 sample using the QIAprep Spin Miniprep Kit (Qiagen) following manufacturer's protocol.

524 sgRNAs were amplified from harvested plasmid DNA using primers For2_sgRNA_Pool
525 and Rev_sgRNA_Pool at 0.6µM in a 50µl PCR reaction with 10µl 5x Q5 buffer and 0.5µl of Q5
526 hot start polymerase, and 1µl 100mM dNTPs (NEB), plus 100ng of the pDNA and UltraPure
527 water. The thermocycler settings were as follows with a heated lid: 98°C for 1min, 14 cycles of
528 98°C for 10sec, 70°C for 20sec, and 72°C for 1min, then finally 72°C for 2min. Barcodes were
529 then introduced with a second round PCR using a legacy Nextera kit of adaptors (Illumina,
530 compatible with FC-121-1031, FC-121-1030, FC-121-1012, FC-121-1011). The second PCR

531 was performed using 1µl of the first PCR product, 4µl UltraPure water (Fisher Scientific), 7.5µl
532 2x NEBNext High Fidelity Master Mix (NEB), and 1.25µl of each barcoded Nextera N5x and
533 N7x index primers per reaction. The thermocycler was set up to hold a heated lid while running
534 at 72ºC for 3min, 98ºC for 2:45min, and 8 cycles of 98ºC for 15sec, 65ºC for 30sec, and 72ºC for
535 1:30min. The desired amplified product is 328nt in length. 5µl samples of the PCR2 products
536 were fractionated on a 2% agarose Tris-Acetate-EDTA (TAE) gel using Sybr Safe dye
537 (Invitrogen) alongside a set amount of 100bp DNA ladder (NEB) and run for 1hr at about 90V
538 for quantification. Samples were imaged and concentrations measured using a BioRad
539 quantitative gel doc system, with quantitation performed using Image J, or dedicated Bio-Rad
540 software so that approximately 100ng of each sample was pooled for sequencing. The samples
541 were PCR column purified (Qiagen) and their final concentrations determined via Nanodrop
542 prior to submission to Tufts University Core Facility of Genomics for sequencing. The pools
543 were sequenced via Illumina HiSeq 2500 SE100 using a legacy Nextera primer mixture.

544 The 5' sequence preceding the 24nt sgRNA was trimmed using Cutadapt (54). Reads
545 were assigned per sgRNA using Python script as described (19). To calculate fitness of the
546 hypomorphs, read counts for each sgRNA were first normalized to the total assigned reads per
547 sample. The sgRNAs with less than 20 cumulative reads at T1 were excluded from analyses in
548 the initial screening but included in the experiments that followed (with T1 counts noted). Any
549 counts of 0 were given a read count of 1 for downstream fitness calculations. Fitness yields from
550 each sgRNA was determined as described (29, 55). Fitness values were normalized to a set of 23
551 shuffle sgRNAs serving as negative/neutral controls by dividing each fitness score by the
552 average fitness of those sgRNAs in each sample. These shuffle sgRNAs were chosen as follows:
553 The median read counts were identified for all shuffle sgRNAs in each replicate sample tested.

554 These median values were then expanded to a range of read counts encompassing the center of
555 the bell-curve generated by plotting read count distributions vs inverse P value. The shuffle
556 sgRNAs that fell in this median range across all replicates and growth conditions in both the WT
557 and GPS strains were selected. Their fitness values were averaged from each sample, and the
558 fitness score yields from all sgRNAs in the pool of that sample were divided by this value.
559 Fitness values of each sgRNA were compared between induced and uninduced conditions
560 (preliminary screening) or between drug treated and untreated samples and the FQR and WT
561 strains where indicated. Multiple t test analyses were employed to identify significant differences
562 in fitness due to growth condition or strain background. The change in fitness generated by each
563 sgRNA due to induction, and the fitness difference of each hypomorph between strains was
564 calculated. Discoveries of fitness scores that significantly differ in these comparisons were
565 determined by the original FDR method of Benjamini and Hochberg with $q < 5\%$ (preliminary
566 screen, (56)) or via the two-stage step-up method of Benjamini, Krieger, and Yekutieli with $Q <$
567 5% (following screens, (30)). Findings characterized as top discoveries were targets represented
568 by 3 or more sgRNAs (those with <10 cumulative reads across replicate cultures at T1 prior to
569 outgrowth as well as ribosomal genes excluded). Data pertaining to the Cipro screen are shown
570 in Supplementary Data 4.

571

572 **Author Contributions**

573 R.R.I and E.H conceptualized and devised the study. E.H and W.H. designed the sgRNA library.
574 I.N and E.H. performed the initial screen. K.N. and E.H. performed and analyzed the WT vs GPS
575 screens in the absence of drug. E.H executed the Cip screen. W.H. tested depletion efficiency of

576 selected sgRNAs. E.G shared all strains, vectors, and methodologies for CRISPRi set up. E.H
577 and R.R.I interpreted the results and wrote the manuscript.

578

579 **Figure legends**

580 **Figure 1: Identification of hypomorphs with reduced fitness in FQR strains.** Diagram for
581 experimental approach and sgRNA library design (Materials & Methods). sgRNAs were
582 designed to target 406 essential genes in *A. baumannii* ("perfect" guides). For each perfect guide,
583 a set of 23 guides with 1 to 2 mismatched nucleotides were created to achieve titratable knock
584 down efficiencies as well as 5 sequence-shuffled guides as negative controls. Additional pool
585 shuffle sgRNAs were made to generate 12,000 guides. Cultures were harvested before (T1) and
586 after (T2) outgrowth with or without drug and dCas9 inducer. Plasmid was extracted and
587 prepared for sequencing to identify hypomorphs with altered fitness under tested conditions.
588 Hypomorph fitness scores were compared between control and experimental groups to determine
589 essential gene targets that generate altered fitness of high-level FQR strains relative to WT. FQ:
590 Fluoroquinolone; FQR: fluoroquinolone resistant; Ciptx: ciprofloxacin treated; Untx: untreated;
591 Ind: induced; using anhydrotetracycline, or aTc.

592

593 **Figure 2: Most sgRNAs with perfect target homology yield low fitness scores.** Volcano plots
594 are displayed to show statistical significance as a function of the change in fitness scores
595 resulting from sgRNA induction (50ng/mL aTc). All symbols refer to unique sgRNAs (light
596 grey). (A): Shuffle sgRNAs that serve as negative controls (mustard yellow) and set used for
597 fitness normalization (bright yellow). (B): The sgRNAs with perfect homology to their target

genome (teal). (C): The sgRNAs with nucleotides most proximal to the 3' PAM site mismatched (purple; 1 to 2 nucleotides upstream). The horizontal dotted line: FDR or Q=5%. (D): Fraction of perfect sgRNAs or mismatched (-1 or -2 to PAM) sgRNAs generating the indicated ranges of fitness (induced vs uninduced). (E, F): The sgRNAs designed for *gyrA* (red, E). S: Shuffle sgRNAs; P: Perfect guide. Positions of mismatched nucleotide in relation to the 3' PAM site, with numbering starting one nucleotide upstream of the PAM site. (E) Display of mean fitness difference of *gyrA* sgRNAs after induction vs. in absence of inducer (dashed line: FDR). (F) Display of *gyrA* data, showing average fitness scores normalized to fitness in the absence of inducer for single and double mutants as well as shuffle sgRNAs.

Figure 3: Relationship between target location in respect to ORF translational start and influence on fitness. (A-C) Statistical significance plotted as a function of fitness differences in the presence and absence of dCas9 induction in WT background (50ng/mL aTc). Light grey circles: all sgRNAs. Black: overlapping with start codon. Red: downstream of start codon. Blue: upstream of start codon. Dotted line: FDR or Q=5%. (D) Distribution of fitness of the various sites chosen.

Figure 4: Outgrowth of banks to 14-16 generations enhances fitness defects. (A, B) Statistical significance plotted as a function of fitness differences after growth for 7-8 generations compared to 14-16 generations in the presence (Black) or absence (Gray) of dCas9 induction (50ng/mL aTc) in WT (A) or GPS (B) backgrounds (50ng/mL aTc). (C-F) Statistical significance plotted as a function of fitness differences after growth for 7-8 generations (C, E)

620 compared to 14-16 generations (D, F) of all hypomorphs upon dCas9 induction. Black: perfect
621 guides. Dark gray: statistically significant sgRNAs passing the FDR or Q=5% via multiple T test
622 analyses. Light gray: sgRNAs not statistically significant. Dotted red box to highlight shifts in
623 fitness that are observed between conditions. WT: Wildtype. GPS: *gyrAparCadeS*.

624

625 **Figure 5: Targets yielding a significant influence on the fitness outcome of the FQR strains.**
626 Fitness of all hypomorphs after outgrowth in the absence or presence of sub-MIC levels of
627 ciprofloxacin (Materials and Methods). Top discoveries uncovered from each comparison are
628 visualized with heat maps showing relative fitness difference scores representative of all
629 respective sgRNAs identified for each target noted. White boxes: depletions not causing change
630 in fitness based on selection parameters. Ciptx: ciprofloxacin treated. Untx: untreated. WT:
631 wildtype. GPL: *gyrAparCadeL*. GPN: *gyrAparCadeN*. GPS: *gyrAparCadeS*.

632

633 **Figure 6: Identifying top discoveries that are in common between the FQR strains.** The
634 Venn diagrams (made at https://bioinformatics.psb.ugent.be/cgi-
635 bin/liste/Venn/calculate_venn.htpl) display number of top discoveries comparing fitness of
636 hypomorphs between the ciprofloxacin treated (Cip) and untreated (Untx) growth conditions (A)
637 and between the FQR strains and the drug susceptible WT strain post Cip exposure (B).
638 Prominent targets are listed which showed a similar phenotype in all 3 or 2/3 FQR vs WT
639 comparisons and which showed up as top discoveries with similar phenotypes in all 3 or 2/3 Cip-
640 Untx comparisons in the FQR strains. Green font: depletion yields a fitness advantage. Blue

641 font: decreased fitness. FQR: Fluoroquinolone resistant. Cip: ciprofloxacin treated. Untx:
642 untreated. WT: wildtype. GPL: *gyrAparCadeL.* GPN: *gyrAparCadeN*. GPS: *gyrAparCadeS*.

643

644 **Figure 7: Opposing effects of translation/ATP generation and LOS biogenesis on the fitness**
645 **of FQR strains in the presence of ciprofloxacin.** (A-C) Statistical significance plotted as a
646 function of fitness score differences between FQR and WT strains or Ciptx and Untx conditions
647 in GPS (A), GPN (B), or GPL (C). Gray: Statistically significant sgRNAs passing the FDR or
648 Q=5% (30). 16 of the prominent targets from the Cip CRISPRi screen are highlighted. Dotted
649 lines: selection parameters wherein substantial changes in fitness are imparted by sgRNAs.
650 Ciptx: ciprofloxacin treated. Untx: untreated. WT: wildtype. GPL: *gyrAparCadeL*. GPN:
651 *gyrAparCadeN*. GPS: *gyrAparCadeS*.

652

653 **Supplementary Figure 1: There is a normal distribution of reads mapped to all sgRNAs.**
654 Bar graphs plot the mean read distribution for all sgRNAs of (A) the original pDNA library prior
655 to introduction into *A. baumannii*, (B) in the WT (wildtype) ATCC 17978UN *A. baumannii*
656 strain background at T1 prior to dCas9 induction, (C) all shuffle sgRNAs also in the WT strain
657 background. Reads were normalized to total mapped reads and transformed. Reads are binned by
658 increments of 10.

659

660 **Supplementary Figure 2: Depletion efficiency of four essential gene targets yielding**
661 **minimal effect on fitness.** Depletion efficiency is noted for each listed target as a percentage
662 against their respective uninduced controls.

663

664 **Supplementary Figure 3: Outgrowth of banks to 14-16 generations does not substantially**
665 **affect fitness of the shuffle guides.** (A-D) Statistical significance plotted as a function of fitness
666 differences after growth for 7-8 generations (A, C) compared to 14-16 generations (B, D) of all
667 hypomorphs upon dCas9 induction. Black: perfect guides. Dark gray: statistically significant
668 sgRNAs passing the FDR or Q=5% via multiple T test analyses. Light gray: sgRNAs not
669 statistically significant. Dotted blue box to visualize shifts in fitness observed. WT: Wildtype.
670 GPS: *gyrAparCadeS*.

671

672 **Supplementary Figure 4: Using additional replicates or generations to identify targets**
673 **specifically important for the fitness of GPS in the absence of drug.** (A,C) Statistical
674 significance plotted as a function of the difference in fitness scores for hypomorphs in GPS vs
675 WT in the absence of drug after growth for 7-8 generations (A, n=10) or 14-16 generations (C,
676 n=5). Of the statistically significant sgRNAs passing the FDR or Q=5% via multiple T test
677 analyses (gray), the targets highlighted showed significant fitness difference scores by at least
678 20% and were represented by at least 3 sgRNAs (excluding ribosomal proteins). Dotted lines:
679 selection parameters wherein substantial changes in fitness are imparted by sgRNAs. (B,D)
680 Scatter plots exhibit the fitness generated by sgRNAs corresponding to targets identified from
681 comparisons between WT (black) and GPS (gray) after 7-8 generations (B) or 14-16 generations
682 (D). The targets noted were similarly identified as in A and C, however these showed significant
683 fitness difference scores of at least 10%. The dotted line marks neutral fitness value of 1. Untx:
684 untreated. WT: Wildtype. GPS: *gyrAparCadeS*.

685

686 **Supplementary Figure 5: Fitness of the unique sgRNA that resulted in the classification of**
687 **top targets having a significant impact on fitness of the FQR strains.** (A) Scatter plots exhibit
688 the fitness generated by sgRNAs corresponding to 16 of the top targets identified from
689 comparisons between WT (black) and GPS (gray) or GPN (red) or GPL (blue) post Cip
690 treatment. The dotted line marks neutral fitness value of 1. (B) Volcano plot shows the
691 significance as a function of the difference in fitness scores of sgRNAs in WT after drug
692 treatment for 7-8 generations vs in absence of drug stress. Top targets identified in the FQR
693 strains causing significantly altered fitness than in the WT strain post Cip exposure are
694 highlighted as described for Figure 7. Gray: Statistically significant sgRNAs passing the FDR or
695 Q=5% via multiple T test analyses (30). The 16 prominent targets from the Cip CRISPRi screen
696 are highlighted. Dotted lines: selection parameters wherein substantial changes in fitness are
697 imparted by sgRNAs. Ciptx: ciprofloxacin treated. Untx: untreated. WT: wildtype. GPL:
698 *gyrAparCadeL*. GPN: *gyrAparCadeN*. GPS: *gyrAparCadeS*.

699

700 **References**

701 1. CDC. 2019. Antibiotic Resistance Threats in the United States. Atlanta, GA: US
702 Department of Health and Human Services, CDC.
703 2. CDC. 2022. COVID-19: U.S. Impact on Antimicrobial Resistance, Special Report 2022.
704 Atlanta, GA: US Department of Health and Human Services, CDC.
705 3. Tacconelli E, Carrara E, Savoldi A, Harbarth S, Mendelson M, Monnet DL, Pulcini C,
706 Kahlmeter G, Kluytmans J, Carmeli Y, Ouellette M, Outterson K, Patel J, Cavaleri M,
707 Cox EM, Houchens CR, Grayson ML, Hansen P, Singh N, Theuretzbacher U, Magrini N,
708 Group WHOPPLW. 2018. Discovery, research, and development of new antibiotics: the
709 WHO priority list of antibiotic-resistant bacteria and tuberculosis. Lancet Infect Dis
710 18:318-327.
711 4. Sun J, Deng Z, Yan A. 2014. Bacterial multidrug efflux pumps: mechanisms, physiology
712 and pharmacological exploitations. Biochem Biophys Res Commun 453:254-67.

713 5. Poole K. 2004. Efflux-mediated multiresistance in Gram-negative bacteria. Clin
714 Microbiol Infect 10:12-26.
715 6. Coyne S, Courvalin P, Perichon B. 2011. Efflux-mediated antibiotic resistance in
716 Acinetobacter spp. Antimicrob Agents Chemother 55:947-53.
717 7. Pagdepanichkit S, Tribuddharat C, Chuanchuen R. 2016. Distribution and expression of
718 the Ade multidrug efflux systems in Acinetobacter baumannii clinical isolates. Can J
719 Microbiol 62:794-801.
720 8. Rumbo C, Gato E, Lopez M, Ruiz de Alegria C, Fernandez-Cuenca F, Martinez-Martinez
721 L, Vila J, Pachon J, Cisneros JM, Rodriguez-Bano J, Pascual A, Bou G, Tomas M,
722 Spanish Group of Nosocomial I, Mechanisms of A, Resistance to A, Spanish Society of
723 Clinical M, Infectious D, Spanish Network for Research in Infectious D. 2013.
724 Contribution of efflux pumps, porins, and beta-lactamases to multidrug resistance in
725 clinical isolates of Acinetobacter baumannii. Antimicrob Agents Chemother 57:5247-57.
726 9. Fernando D, Zhanel G, Kumar A. 2013. Antibiotic resistance and expression of
727 resistance-nodulation-division pump- and outer membrane porin-encoding genes in
728 Acinetobacter species isolated from Canadian hospitals. Can J Infect Dis Med Microbiol
729 24:17-21.
730 10. Geisinger E, Vargas-Cuebas G, Mortman NJ, Syal S, Dai Y, Wainwright EL, Lazinski D,
731 Wood S, Zhu Z, Anthony J, van Opijnen T, Isberg RR. 2019. The Landscape of
732 Phenotypic and Transcriptional Responses to Ciprofloxacin in Acinetobacter baumannii:
733 Acquired Resistance Alleles Modulate Drug-Induced SOS Response and Prophage
734 Replication. mBio 10.
735 11. Naidu V, Bartczak A, Brzoska AJ, Lewis P, Eijkelkamp BA, Paulsen IT, Elbourne LDH,
736 Hassan KA. 2023. Evolution of RND efflux pumps in the development of a successful
737 pathogen. Drug Resist Updat 66:100911.
738 12. Magnet S, Courvalin P, Lambert T. 2001. Resistance-nodulation-cell division-type efflux
739 pump involved in aminoglycoside resistance in Acinetobacter baumannii strain BM4454.
740 Antimicrob Agents Chemother 45:3375-80.
741 13. Coyne S, Rosenfeld N, Lambert T, Courvalin P, Perichon B. 2010. Overexpression of
742 resistance-nodulation-cell division pump AdeFGH confers multidrug resistance in
743 Acinetobacter baumannii. Antimicrob Agents Chemother 54:4389-93.
744 14. Yoon EJ, Chabane YN, Goussard S, Snesrud E, Courvalin P, De E, Grillot-Courvalin C.
745 2015. Contribution of resistance-nodulation-cell division efflux systems to antibiotic
746 resistance and biofilm formation in Acinetobacter baumannii. mBio 6.
747 15. Rosenfeld N, Bouchier C, Courvalin P, Perichon B. 2012. Expression of the resistance-
748 nodulation-cell division pump AdeIJK in Acinetobacter baumannii is regulated by AdeN,
749 a TetR-type regulator. Antimicrob Agents Chemother 56:2504-10.
750 16. Hamami E, Huo W, Castaneda A, Bai J, Syal S, Ortiz-Marquez JC, Opijnen Tv,
751 Geisinger E, Isberg RR. 2023. Identification of Determinants that Allow Maintenance of
752 High-Level Fluoroquinolone Resistance in Acinetobacter baumannii.
753 bioRxiv doi:10.1101/2023.10.03.560562:2023.10.03.560562.
754 17. Hooppaw AJ, McGuffey JC, Di Venanzio G, Ortiz-Marquez JC, Weber BS, Lightly TJ,
755 van Opijnen T, Scott NE, Cardona ST, Feldman MF. 2022. The Phenylacetic Acid
756 Catabolic Pathway Regulates Antibiotic and Oxidative Stress Responses in
757 Acinetobacter. mBio 13:e0186321.

758 18. Jost M, Santos DA, Saunders RA, Horlbeck MA, Hawkins JS, Scaria SM, Norman TM,
759 Hussmann JA, Liem CR, Gross CA, Weissman JS. 2020. Titrating gene expression using
760 libraries of systematically attenuated CRISPR guide RNAs. Nat Biotechnol 38:355-364.
761 19. Hawkins JS, Silvis MR, Koo BM, Peters JM, Osadnik H, Jost M, Hearne CC, Weissman
762 JS, Todor H, Gross CA. 2020. Mismatch-CRISPRi Reveals the Co-varying Expression-
763 Fitness Relationships of Essential Genes in Escherichia coli and Bacillus subtilis. Cell
764 Syst 11:523-535 e9.
765 20. Rousset F, Cui L, Siouve E, Becavin C, Depardieu F, Bikard D. 2018. Genome-wide
766 CRISPR-dCas9 screens in E. coli identify essential genes and phage host factors. PLoS
767 Genet 14:e1007749.
768 21. Ward RD, Tran JS, Banta AB, Bacon EE, Rose WE, Peters JM. 2023. Essential Gene
769 Knockdowns Reveal Genetic Vulnerabilities and Antibiotic Sensitivities in Acinetobacter
770 baumannii. bioRxiv doi:10.1101/2023.08.02.551708.
771 22. Geisinger E, Mortman NJ, Dai Y, Cokol M, Syal S, Farinha A, Fisher DG, Tang AY,
772 Lazinski DW, Wood S, Anthony J, van Opijnen T, Isberg RR. 2020. Antibiotic
773 susceptibility signatures identify potential antimicrobial targets in the Acinetobacter
774 baumannii cell envelope. Nat Commun 11:4522.
775 23. Peters JM, Koo BM, Patino R, Heussler GE, Hearne CC, Qu J, Inclan YF, Hawkins JS,
776 Lu CHS, Silvis MR, Harden MM, Osadnik H, Peters JE, Engel JN, Dutton RJ, Grossman
777 AD, Gross CA, Rosenberg OS. 2019. Enabling genetic analysis of diverse bacteria with
778 Mobile-CRISPRi. Nat Microbiol 4:244-250.
779 24. Bai J, Dai Y, Farinha A, Tang AY, Syal S, Vargas-Cuebas G, van Opijnen T, Isberg RR,
780 Geisinger E. 2021. Essential Gene Analysis in Acinetobacter baumannii by High-Density
781 Transposon Mutagenesis and CRISPR Interference. J Bacteriol 203:e0056520.
782 25. DeJesus MA, Ambadipudi C, Baker R, Sassetti C, Ioerger TR. 2015. TRANSIT--A
783 Software Tool for Himar1 TnSeq Analysis. PLoS Comput Biol 11:e1004401.
784 26. DeJesus MA, Zhang YJ, Sassetti CM, Rubin EJ, Sacchettini JC, Ioerger TR. 2013.
785 Bayesian analysis of gene essentiality based on sequencing of transposon insertion
786 libraries. Bioinformatics 29:695-703.
787 27. Gallagher LA, Ramage E, Weiss EJ, Radey M, Hayden HS, Held KG, Huse HK,
788 Zurawski DV, Brittnacher MJ, Manoil C. 2015. Resources for Genetic and Genomic
789 Analysis of Emerging Pathogen Acinetobacter baumannii. J Bacteriol 197:2027-35.
790 28. Wang N, Ozer EA, Mandel MJ, Hauser AR. 2014. Genome-wide identification of
791 Acinetobacter baumannii genes necessary for persistence in the lung. mBio 5:e01163-14.
792 29. van Opijnen T, Bodi KL, Camilli A. 2009. Tn-seq: high-throughput parallel sequencing
793 for fitness and genetic interaction studies in microorganisms. Nat Methods 6:767-72.
794 30. Benjamini Y, Krieger, A. M., & Yekutieli, D. 2006. Adaptive linear step-up procedures
795 that control the false discovery rate. Biometrika 93:491-507.
796 31. Yakhnin AV, Bubunenko M, Mandell ZF, Lubkowska L, Husher S, Babitzke P, Kashlev
797 M. 2023. Robust regulation of transcription pausing in Escherichia coli by the ubiquitous
798 elongation factor NusG. Proc Natl Acad Sci U S A 120:e2221114120.
799 32. Baniulyte G, Singh N, Benoit C, Johnson R, Ferguson R, Paramo M, Stringer AM, Scott
800 A, Lapierre P, Wade JT. 2017. Identification of regulatory targets for the bacterial Nus
801 factor complex. Nat Commun 8:2027.

802 33. Schemidt RA, Qu J, Williams JR, Brusilow WS. 1998. Effects of carbon source on
803 expression of F0 genes and on the stoichiometry of the c subunit in the F1F0 ATPase of
804 Escherichia coli. J Bacteriol 180:3205-8.
805 34. Xu Q, Guo M, Yu F. 2023. beta-Barrel Assembly Machinery (BAM) Complex as Novel
806 Antibacterial Drug Target. Molecules 28.
807 35. Sugawara E, Nikaido H. 2014. Properties of AdeABC and AdeIJK efflux systems of
808 Acinetobacter baumannii compared with those of the AcrAB-TolC system of Escherichia
809 coli. Antimicrob Agents Chemother 58:7250-7.
810 36. Ruiz N, Gronenberg LS, Kahne D, Silhavy TJ. 2008. Identification of two inner-
811 membrane proteins required for the transport of lipopolysaccharide to the outer
812 membrane of Escherichia coli. Proc Natl Acad Sci U S A 105:5537-42.
813 37. Sperandeo P, Cescutti R, Villa R, Di Benedetto C, Candia D, Deho G, Polissi A. 2007.
814 Characterization of lptA and lptB, two essential genes implicated in lipopolysaccharide
815 transport to the outer membrane of Escherichia coli. J Bacteriol 189:244-53.
816 38. Powers MJ, Trent MS. 2018. Phospholipid retention in the absence of asymmetry
817 strengthens the outer membrane permeability barrier to last-resort antibiotics. Proc Natl
818 Acad Sci U S A 115:E8518-E8527.
819 39. Simpson BW, Nieckarz M, Pinedo V, McLean AB, Cava F, Trent MS. 2021.
820 Acinetobacter baumannii Can Survive with an Outer Membrane Lacking
821 Lipooligosaccharide Due to Structural Support from Elongasome Peptidoglycan
822 Synthesis. mBio 12:e0309921.
823 40. Boll JM, Crofts AA, Peters K, Cattoir V, Vollmer W, Davies BW, Trent MS. 2016. A
824 penicillin-binding protein inhibits selection of colistin-resistant, lipooligosaccharide-
825 deficient Acinetobacter baumannii. Proc Natl Acad Sci U S A 113:E6228-E6237.
826 41. Arunmanee W, Pathania M, Solovyova AS, Le Brun AP, Ridley H, Basle A, van den
827 Berg B, Lakey JH. 2016. Gram-negative trimeric porins have specific LPS binding sites
828 that are essential for porin biogenesis. Proc Natl Acad Sci U S A 113:E5034-43.
829 42. Webby MN, Oluwole AO, Pedebos C, Inns PG, Olerinyova A, Prakaash D, Housden NG,
830 Benn G, Sun D, Hoogenboom BW, Kukura P, Mohammed S, Robinson CV, Khalid S,
831 Kleanthous C. 2022. Lipids mediate supramolecular outer membrane protein assembly in
832 bacteria. Sci Adv 8:eadc9566.
833 43. Sielaff H, Duncan TM, Borsch M. 2018. The regulatory subunit epsilon in Escherichia
834 coli F(O)F(1)-ATP synthase. Biochim Biophys Acta Bioenerg 1859:775-788.
835 44. Guo H, Courbon GM, Bueler SA, Mai J, Liu J, Rubinstein JL. 2021. Structure of
836 mycobacterial ATP synthase bound to the tuberculosis drug bedaquiline. Nature 589:143-
837 147.
838 45. Saw WG, Le KCM, Shin J, Kwek JHM, Wong CF, Ragunathan P, Fong TC, Muller V,
839 Gruber G. 2023. Atomic insights of an up and down conformation of the Acinetobacter
840 baumannii F(1) -ATPase subunit epsilon and deciphering the residues critical for ATP
841 hydrolysis inhibition and ATP synthesis. FASEB J 37:e23040.
842 46. Sobti M, Walshe JL, Wu D, Ishmukhametov R, Zeng YC, Robinson CV, Berry RM,
843 Stewart AG. 2020. Cryo-EM structures provide insight into how E. coli F(1)F(o) ATP
844 synthase accommodates symmetry mismatch. Nat Commun 11:2615.
845 47. Demmer JK, Phillips BP, Uhrig OL, Filloux A, Allsopp LP, Bublitz M, Meier T. 2022.
846 Structure of ATP synthase from ESKAPE pathogen Acinetobacter baumannii. Sci Adv
847 8:eabl5966.

848 48. Koumandou VL, Kossida S. 2014. Evolution of the F0F1 ATP synthase complex in light
849 of the patchy distribution of different bioenergetic pathways across prokaryotes. PLoS
850 Comput Biol 10:e1003821.
851 49. Liu J, Hicks DB, Krulwich TA. 2013. Roles of AtpI and two YidC-type proteins from
852 alkaliphilic Bacillus pseudofirmus OF4 in ATP synthase assembly and nonfermentative
853 growth. J Bacteriol 195:220-30.
854 50. Manuse S, Shan Y, Canas-Duarte SJ, Bakshi S, Sun WS, Mori H, Paulsson J, Lewis K.
855 2021. Bacterial persisters are a stochastically formed subpopulation of low-energy cells.
856 PLoS Biol 19:e3001194.
857 51. Shan Y, Brown Gandt A, Rowe SE, Deisinger JP, Conlon BP, Lewis K. 2017. ATP-
858 Dependent Persister Formation in Escherichia coli. mBio 8.
859 52. El Meouche I, Dunlop MJ. 2018. Heterogeneity in efflux pump expression predisposes
860 antibiotic-resistant cells to mutation. Science 362:686-690.
861 53. Huo W, Busch LM, Hernandez-Bird J, Hamami E, Marshall CW, Geisinger E, Cooper
862 VS, van Opijnen T, Rosch JW, Isberg RR. 2022. Immunosuppression broadens
863 evolutionary pathways to drug resistance and treatment failure during Acinetobacter
864 baumannii pneumonia in mice. Nat Microbiol 7:796-809.
865 54. Martin M. 2011. Cutadapt removes adapter sequences from high-throughput sequencing
866 reads. 2011 17:3.
867 55. van Opijnen T, Camilli A. 2013. Transposon insertion sequencing: a new tool for
868 systems-level analysis of microorganisms. Nat Rev Microbiol 11:435-42.
869 56. Benjamini Y, & Hochberg, Y. 1995. Controlling the false discovery rate: a practical and
870 powerful approach to multiple testing. Journal of the Royal Statistical Society Series B
871 (Methodological):289-300.

872

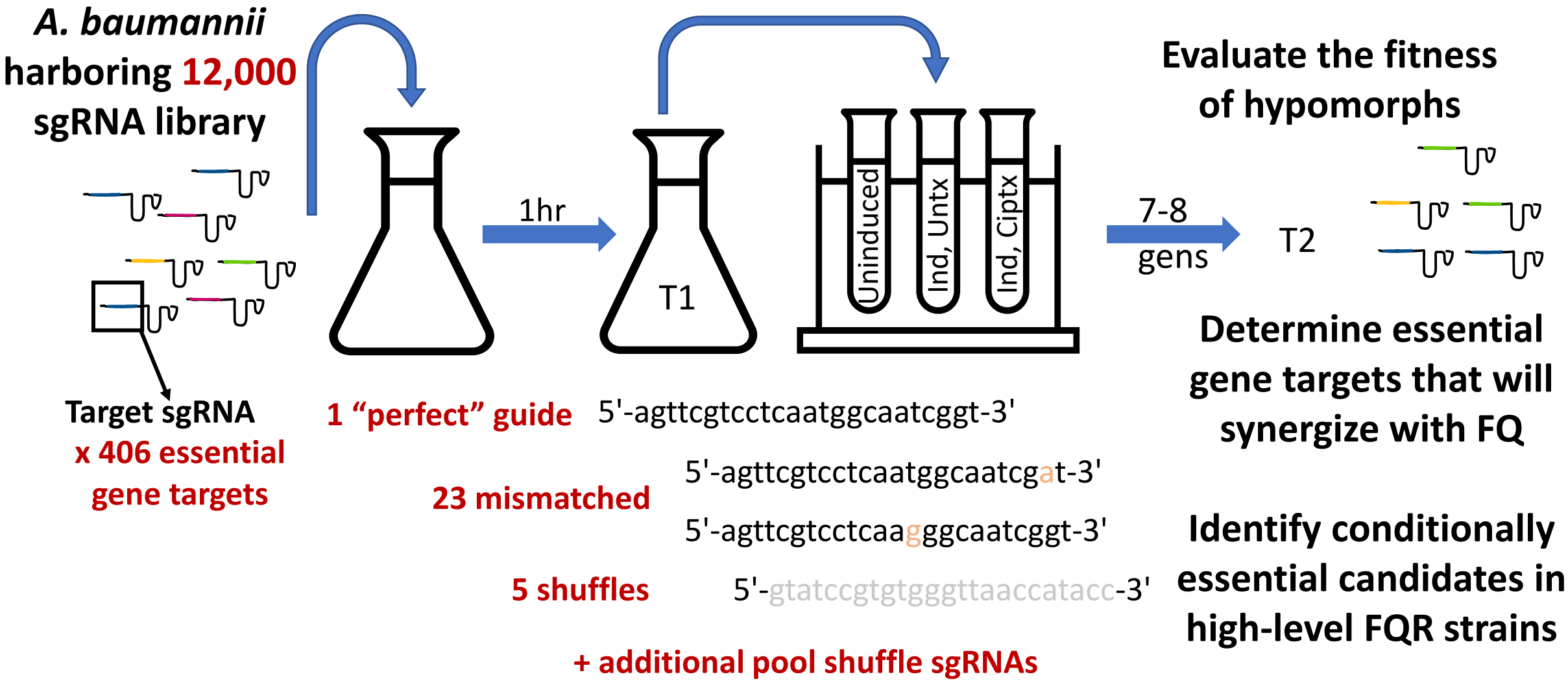
A. baumannii harboring 12,000 sgRNA library
Target sgRNA x 406 essential gene targets
1hr
T1
Uninduced
Ind, Untx
Ind, Ciptx
7-8 gens
T2
Evaluate the fitness of hypomorphs
Determine essential gene targets that will synergize with FQ
Identify conditionally essential candidates in high-level FQR strains
1 "perfect" guide
5'-agttcgtcctcaatggcaatcggt-3'
23 mismatched
5'-agttcgtcctcaatggcaatcgat-3'
5'-agttcgtcctcaagggcaatcggt-3'
5 shuffles
5'-gtatccgtgtgggttaaccatacc-3'
+ additional pool shuffle sgRNAs

Fig 1

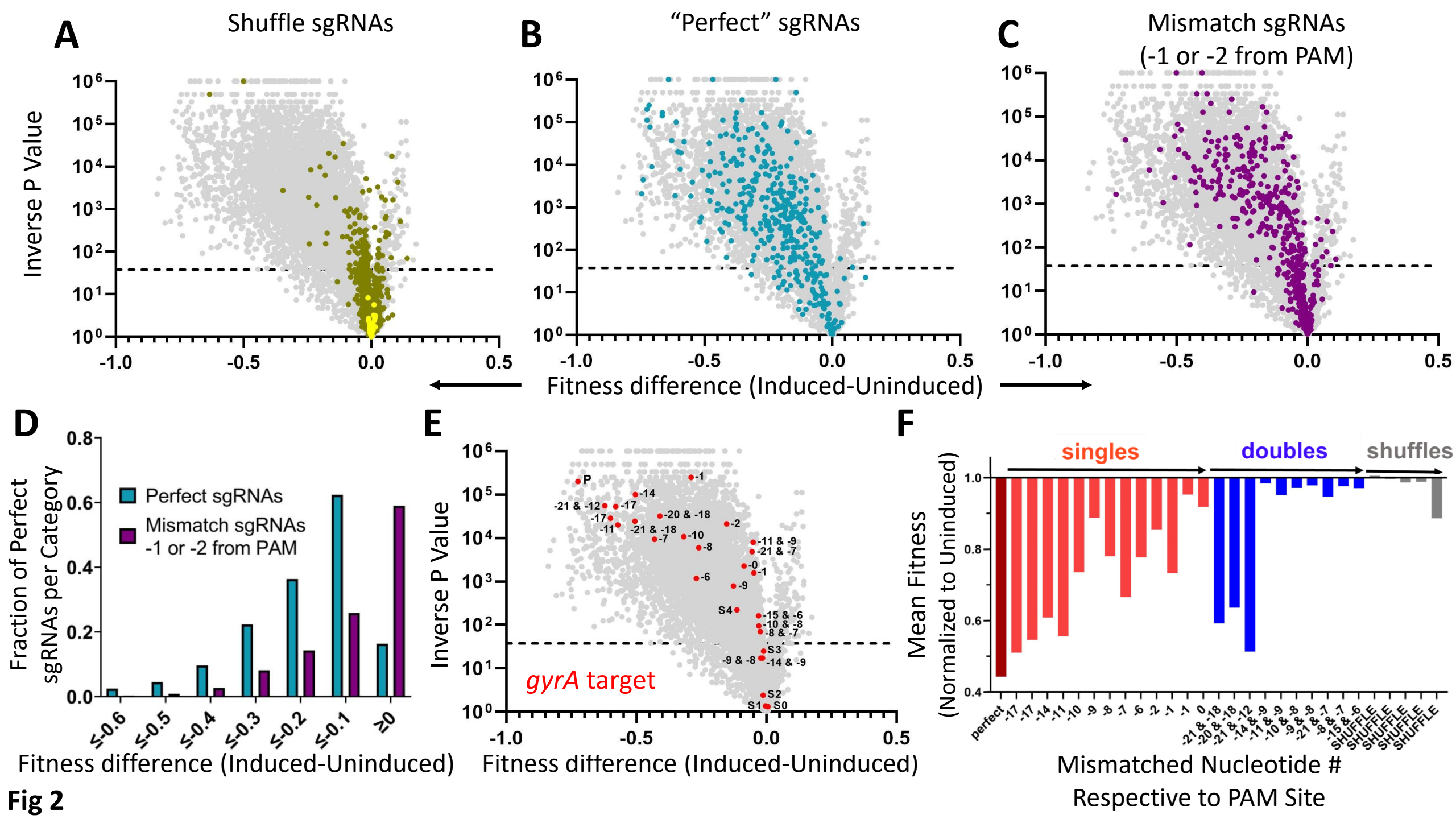
A
Shuffle sgRNAs
B
"Perfect" sgRNAs
C
Mismatch sgRNAs
(-1 or -2 from PAM)
Inverse P Value
Fitness difference (Induced-Uninduced)
D
Fraction of Perfect sgRNAs per Category
Perfect sgRNAs
Mismatch sgRNAs
-1 or -2 from PAM
≤-0.6
≤-0.5
≤-0.4
≤-0.3
≤-0.2
≤-0.1
≥0
Fitness difference (Induced-Uninduced)
E
gyrA target
Fitness difference (Induced-Uninduced)
F
singles
doubles
shuffles
Mean Fitness
(Normalized to Uninduced)
Mismatched Nucleotide #
Respective to PAM Site

Fig 2

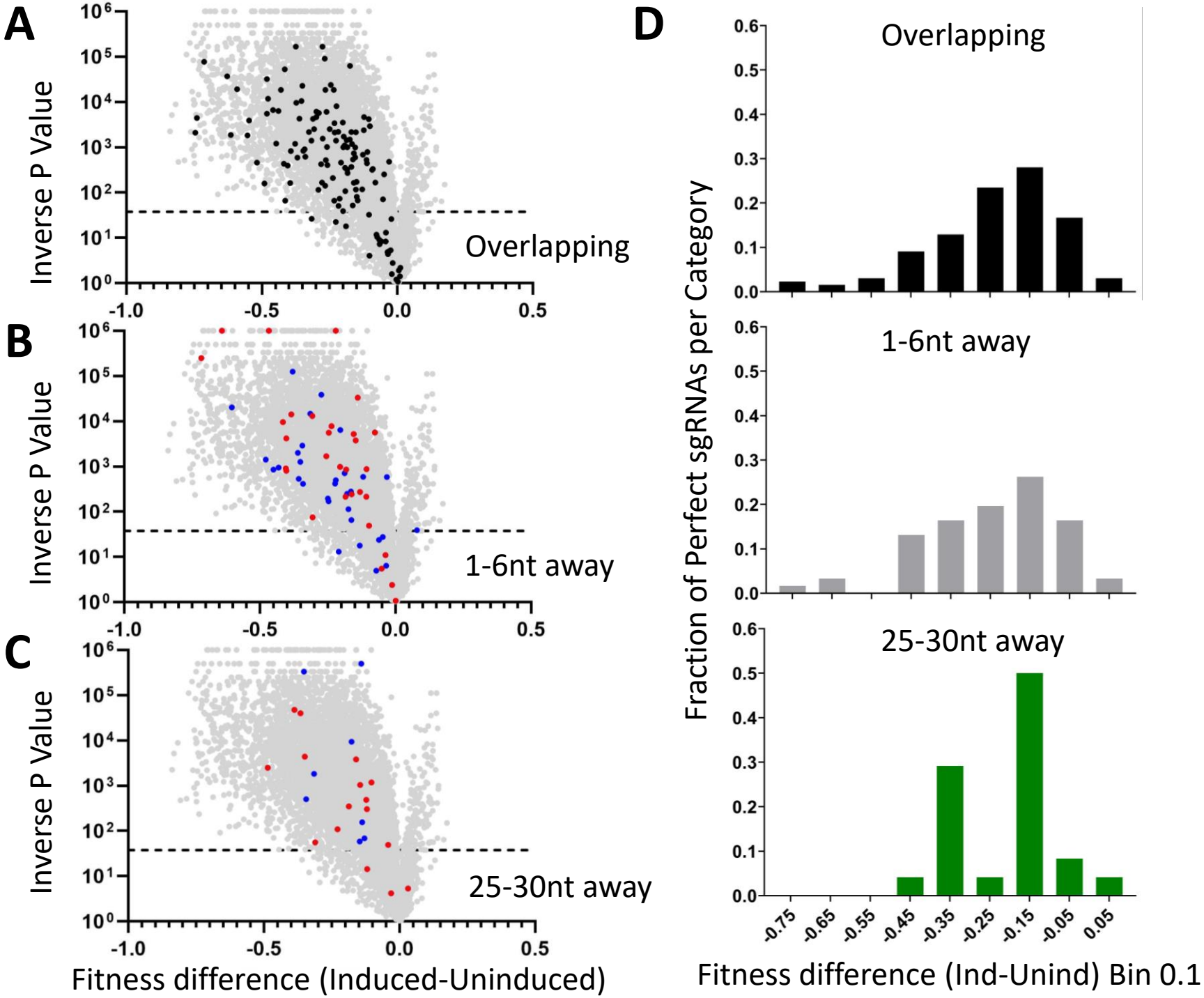
A
B
C
D
Inverse P Value
Overlapping
1-6nt away
25-30nt away
Fitness difference (Induced-Uninduced)
Fraction of Perfect sgRNAs per Category
Fitness difference (Ind-Unind) Bin 0.1

Fig 3

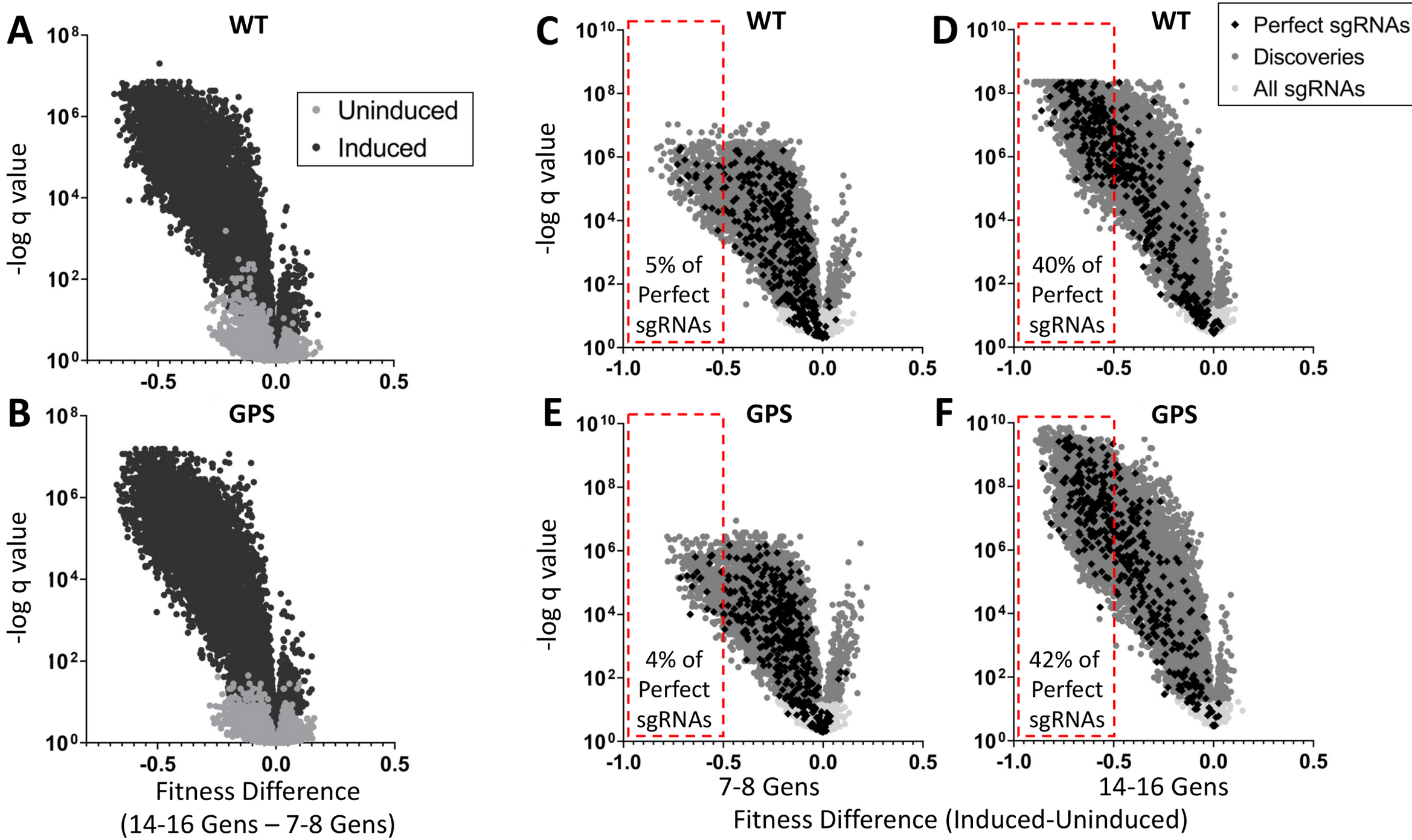
A
WT
Uninduced
Induced
-log q value
B
GPS
Fitness Difference
(14-16 Gens – 7-8 Gens)
C
WT
5% of
Perfect
sgRNAs
D
WT
40% of
Perfect
sgRNAs
Perfect sgRNAs
Discoveries
All sgRNAs
E
GPS
4% of
Perfect
sgRNAs
7-8 Gens
F
GPS
42% of
Perfect
sgRNAs
14-16 Gens
Fitness Difference (Induced-Uninduced)

Fig 4

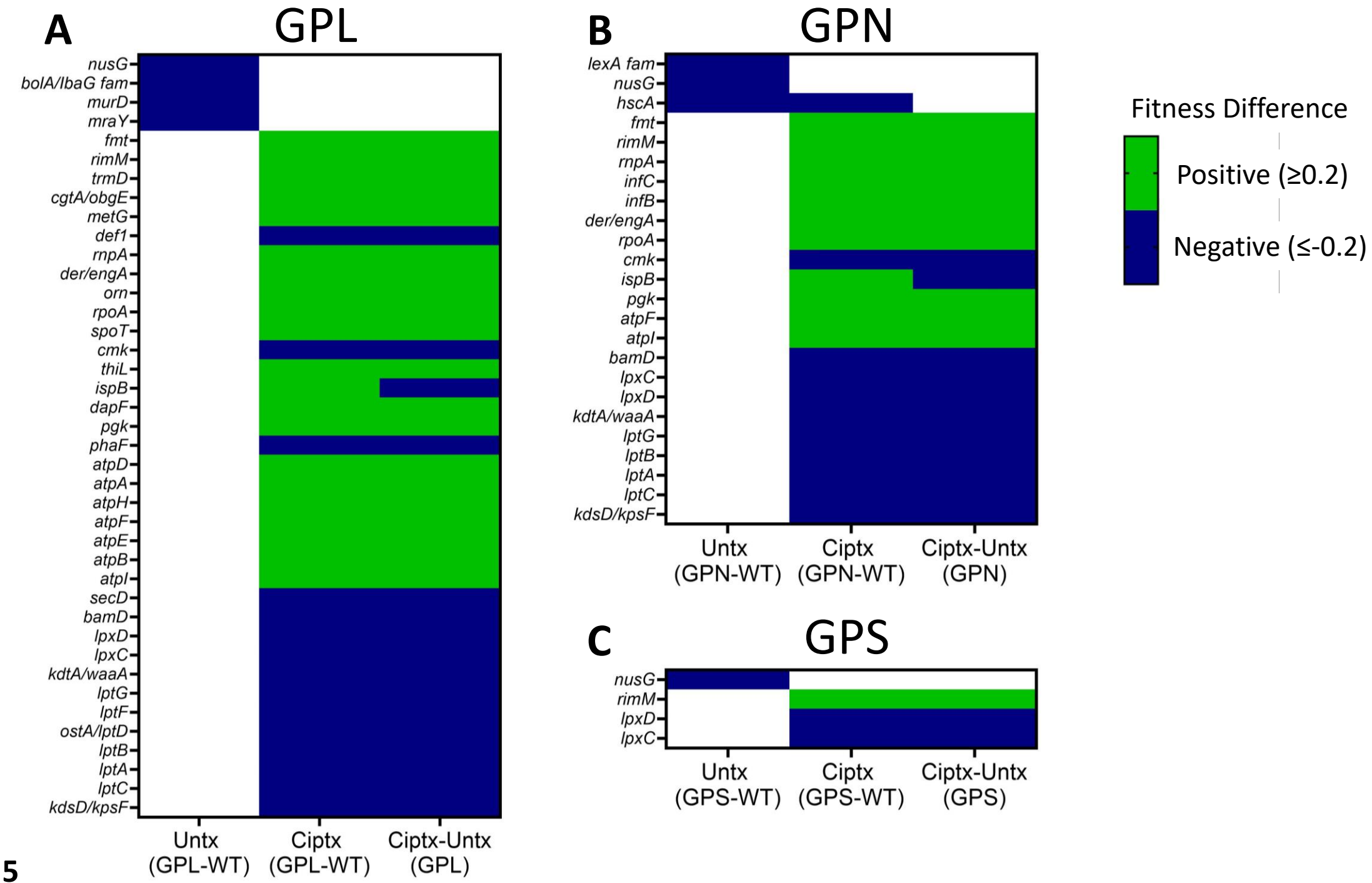
A
GPL
nusG
bolA/IbaG fam
murD
mraY
fmt
rimM
trmD
cgtA/obgE
metG
def1
rnpA
der/engA
orn
rpoA
spoT
cmk
thiL
ispB
dapF
pgk
phaF
atpD
atpA
atpH
atpF
atpE
atpB
atpI
secD
bamD
lpxD
lpxC
kdtA/waaA
lptG
lptF
ostA/lptD
lptB
lptA
lptC
kdsD/kpsF
Untx (GPL-WT)
Ciptx (GPL-WT)
Ciptx-Untx (GPL)
B
GPN
lexA fam
nusG
hscA
fmt
rimM
rnpA
infC
infB
der/engA
rpoA
cmk
ispB
pgk
atpF
atpI
bamD
lpxC
lpxD
kdtA/waaA
lptG
lptB
lptA
lptC
kdsD/kpsF
Untx (GPN-WT)
Ciptx (GPN-WT)
Ciptx-Untx (GPN)
C
GPS
nusG
rimM
lpxD
lpxC
Untx (GPS-WT)
Ciptx (GPS-WT)
Ciptx-Untx (GPS)
Fitness Difference
Positive (≥0.2)
Negative (≤-0.2)

Fig 5

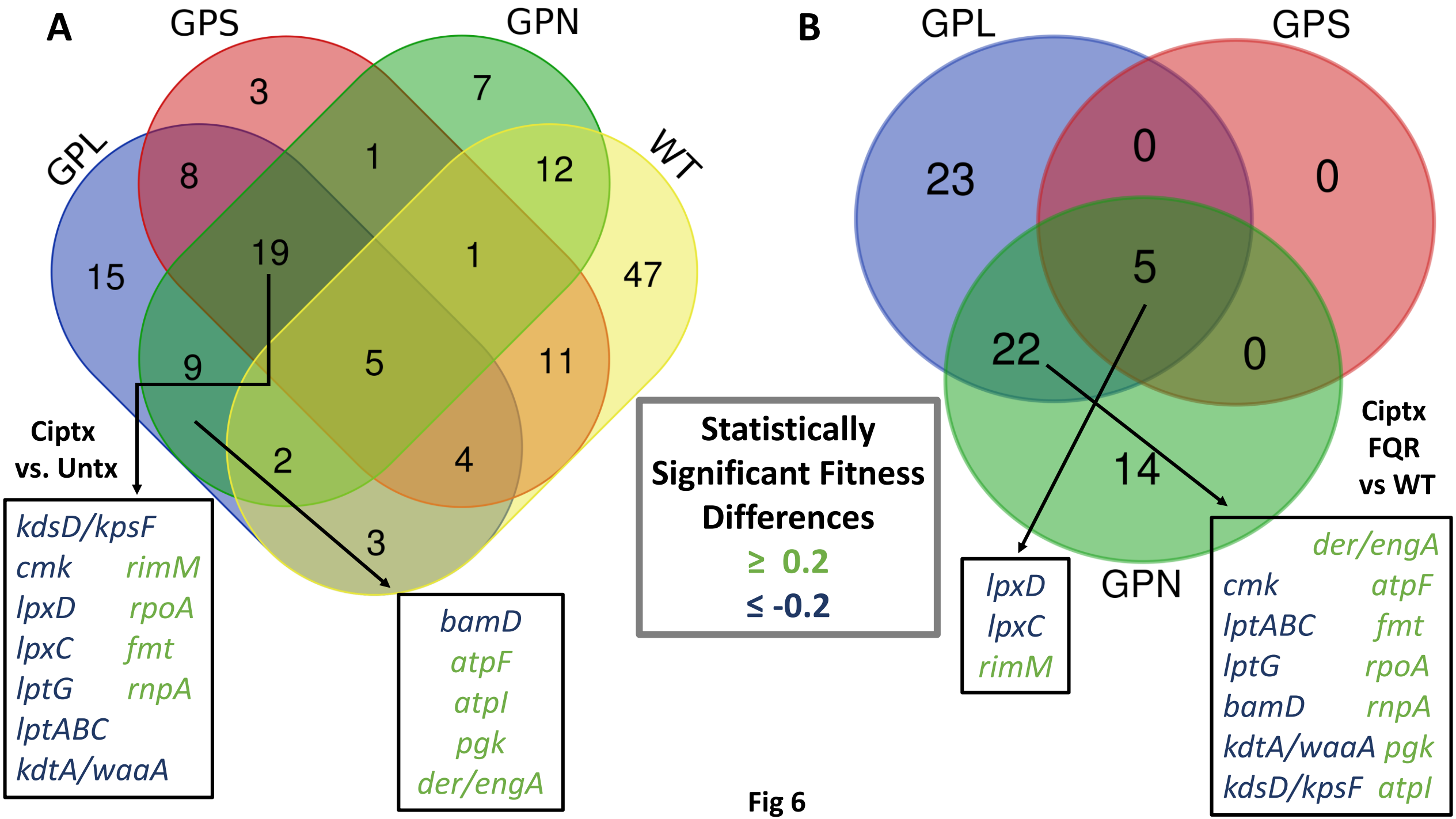
A
GPS
GPN
GPL
WT
3
7
8
1
12
15
19
1
47
9
5
11
2
4
3
Ciptx
vs. Untx
kdsD/kpsF
cmk
rimM
lpxD
rpoA
lpxC
fmt
lptG
rnpA
lptABC
kdtA/waaA
bamD
atpF
atpI
pgk
der/engA
Statistically
Significant Fitness
Differences
≥ 0.2
≤ -0.2
B
GPL
GPS
23
0
0
5
22
0
14
GPN
Ciptx
FQR
vs WT
lpxD
lpxC
rimM
der/engA
cmk
atpF
lptABC
fmt
lptG
rpoA
bamD
rnpA
kdtA/waaA
pgk
kdsD/kpsF
atpI

Fig 6

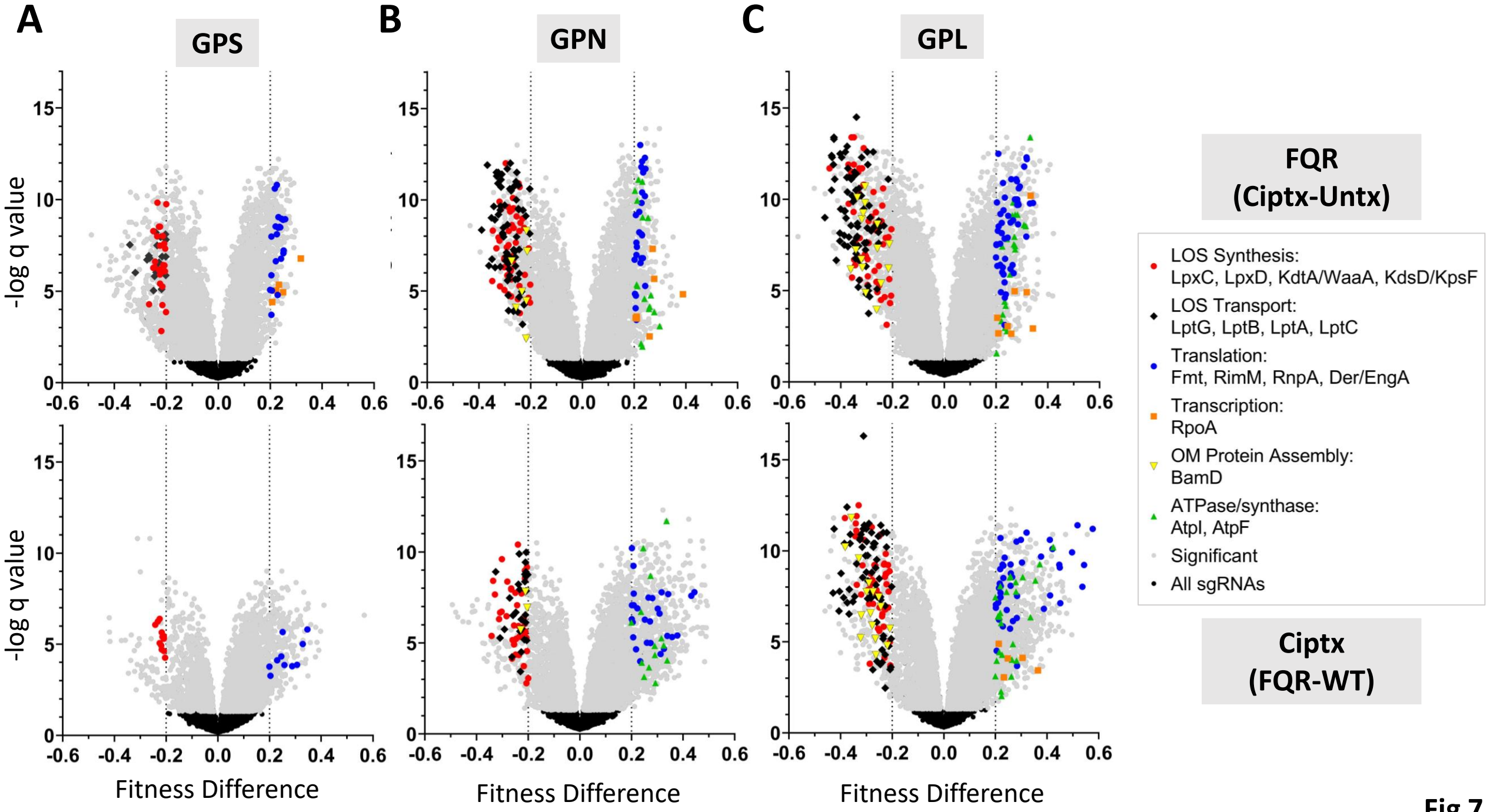
A
GPS
B
GPN
C
GPL
-log q value
Fitness Difference
FQR
(Ciptx-Untx)
Ciptx
(FQR-WT)
LOS Synthesis:
LpxC, LpxD, KdtA/WaaA, KdsD/KpsF
LOS Transport:
LptG, LptB, LptA, LptC
Translation:
Fmt, RimM, RnpA, Der/EngA
Transcription:
RpoA
OM Protein Assembly:
BamD
ATPase/synthase:
AtpI, AtpF
Significant
All sgRNAs

Fig 7

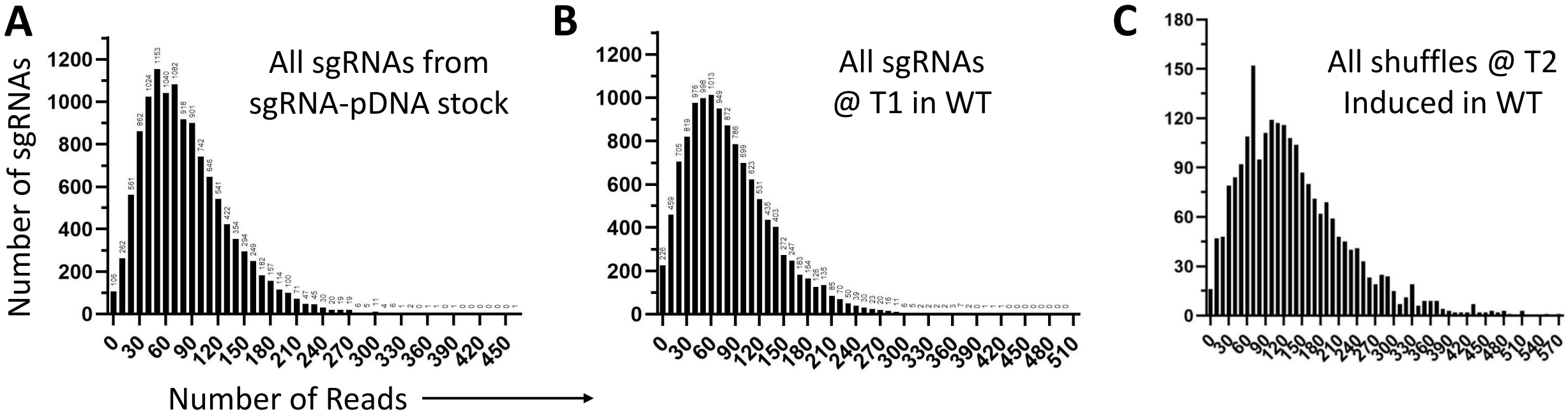
A
All sgRNAs from
sgRNA-pDNA stock
Number of sgRNAs
Number of Reads
B
All sgRNAs
@ T1 in WT
C
All shuffles @ T2
Induced in WT

Supp Fig 1

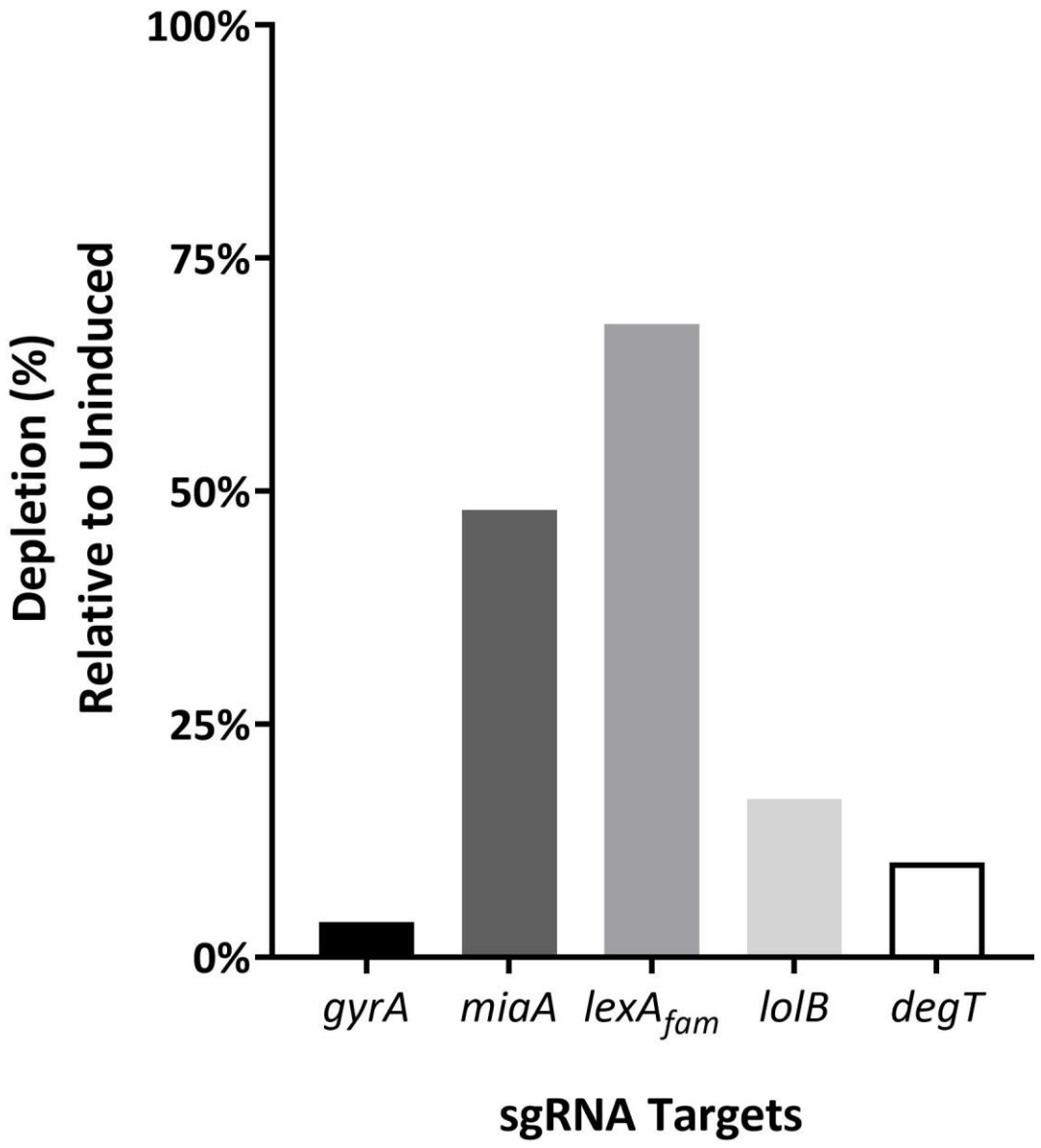
100%
75%
50%
25%
0%
Depletion (%)
Relative to Uninduced
gyrA
miaA
lexA fam
lolB
degT
sgRNA Targets

Supp Fig 2

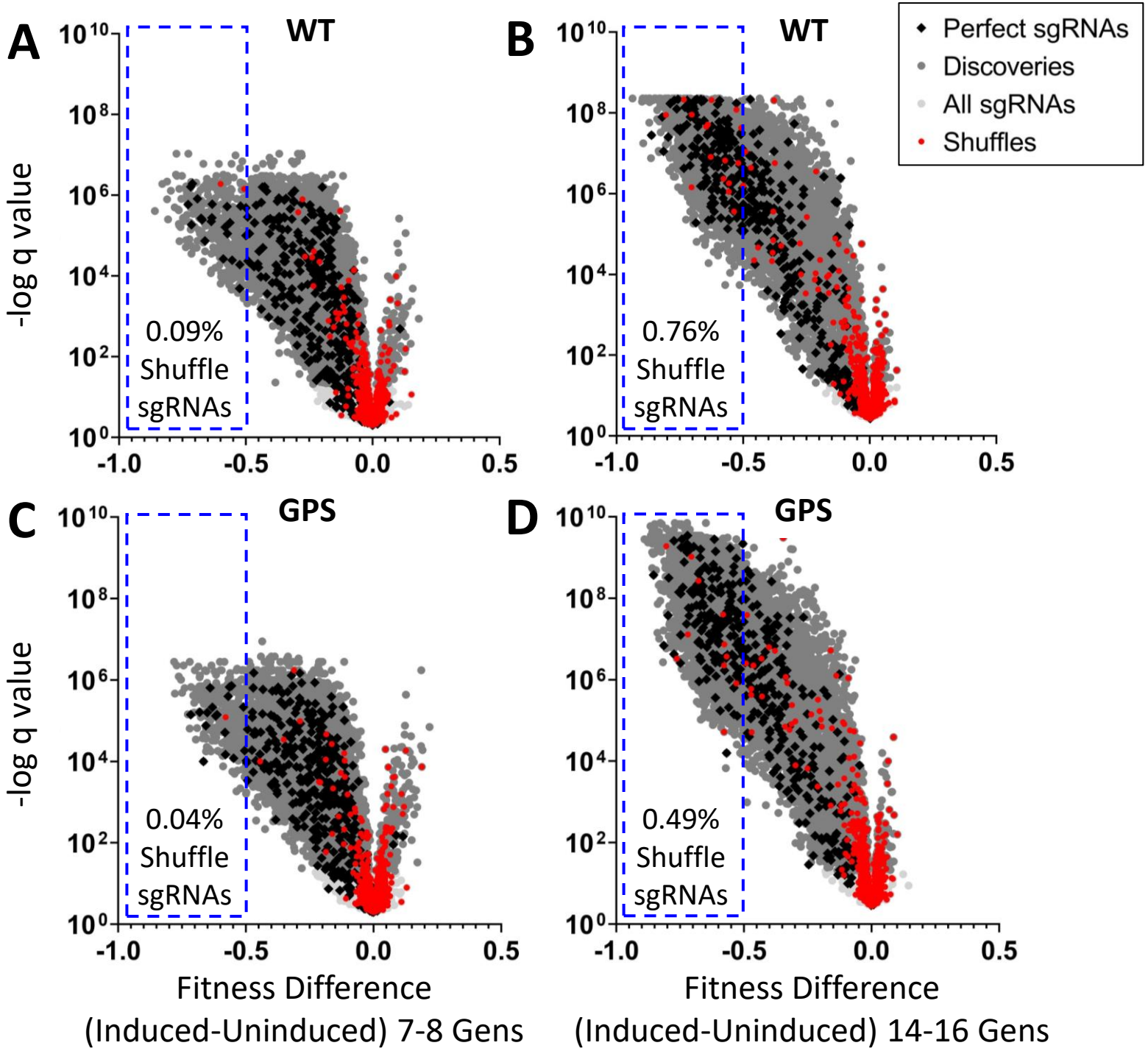
A
WT
B
WT
C
GPS
D
GPS
Perfect sgRNAs
Discoveries
All sgRNAs
Shuffles
-log q value
0.09% Shuffle sgRNAs
0.76% Shuffle sgRNAs
0.04% Shuffle sgRNAs
0.49% Shuffle sgRNAs
Fitness Difference (Induced-Uninduced) 7-8 Gens
Fitness Difference (Induced-Uninduced) 14-16 Gens

Supp Fig 3

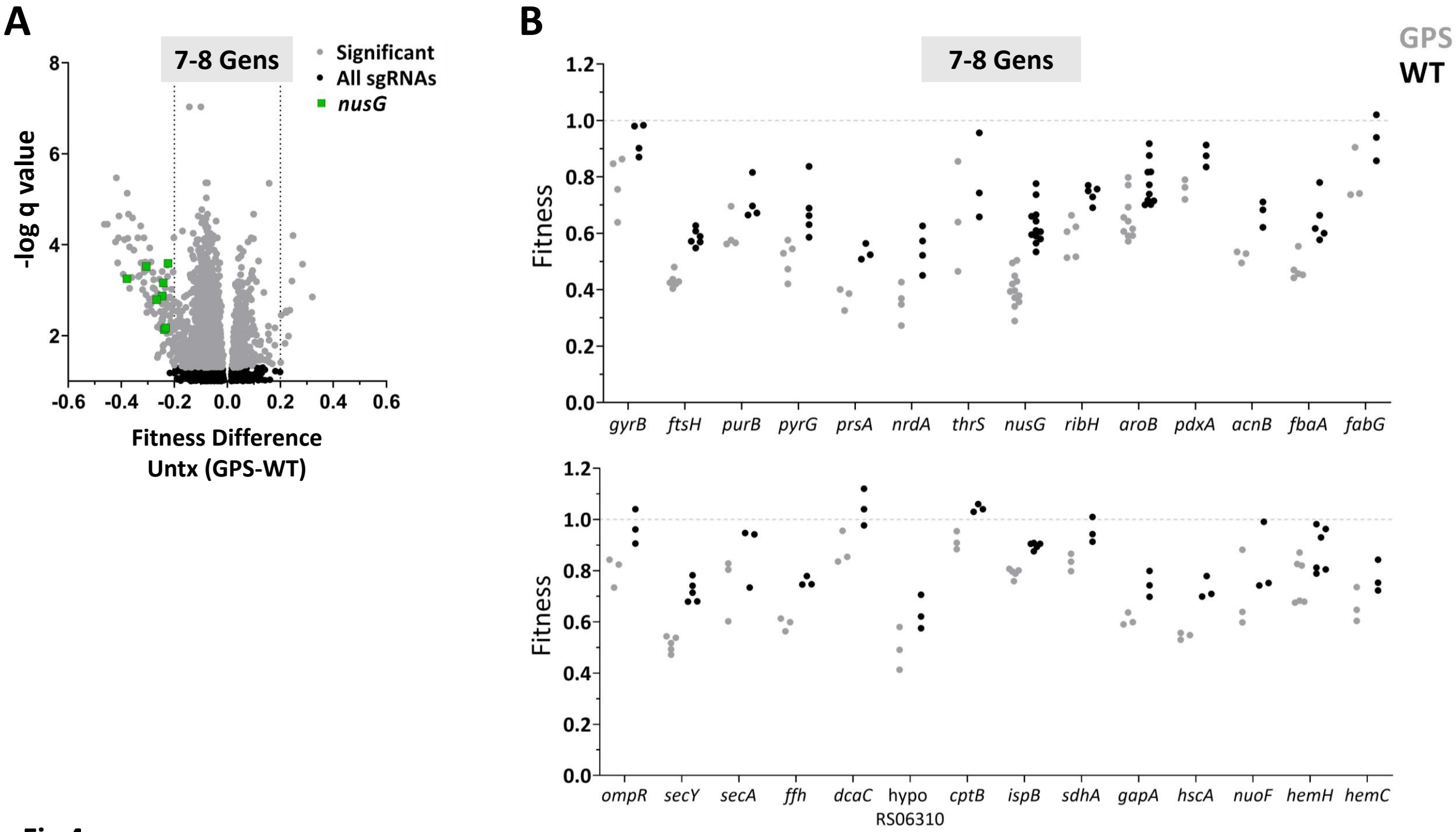
A
7-8 Gens
Significant
All sgRNAs
nusG
-log q value
Fitness Difference
Untx (GPS-WT)
B
7-8 Gens
GPS
WT
Fitness
gyrB
ftsH
purB
pyrG
prsA
nrdA
thrS
nusG
ribH
aroB
pdxA
acnB
fbaA
fabG
ompR
secY
secA
ffh
dcaC
hypo RS06310
cptB
ispB
sdhA
gapA
hscA
nuoF
hemH
hemC

Supp Fig 4

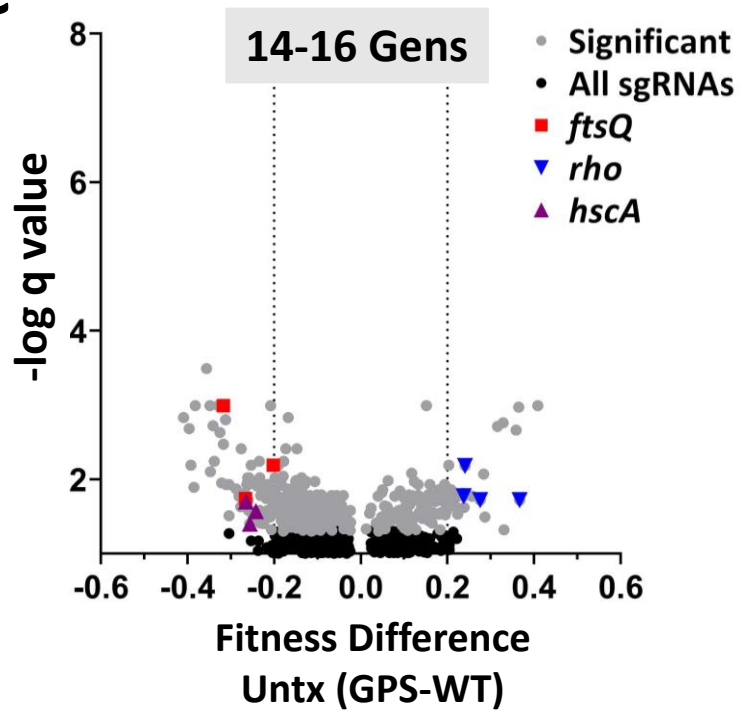
C
14-16 Gens
Significant
All sgRNAs
ftsQ
rho
hscA
-log q value
8
6
4
2
-0.6
-0.4
-0.2
0.0
0.2
0.4
0.6
Fitness Difference
Untx (GPS-WT)

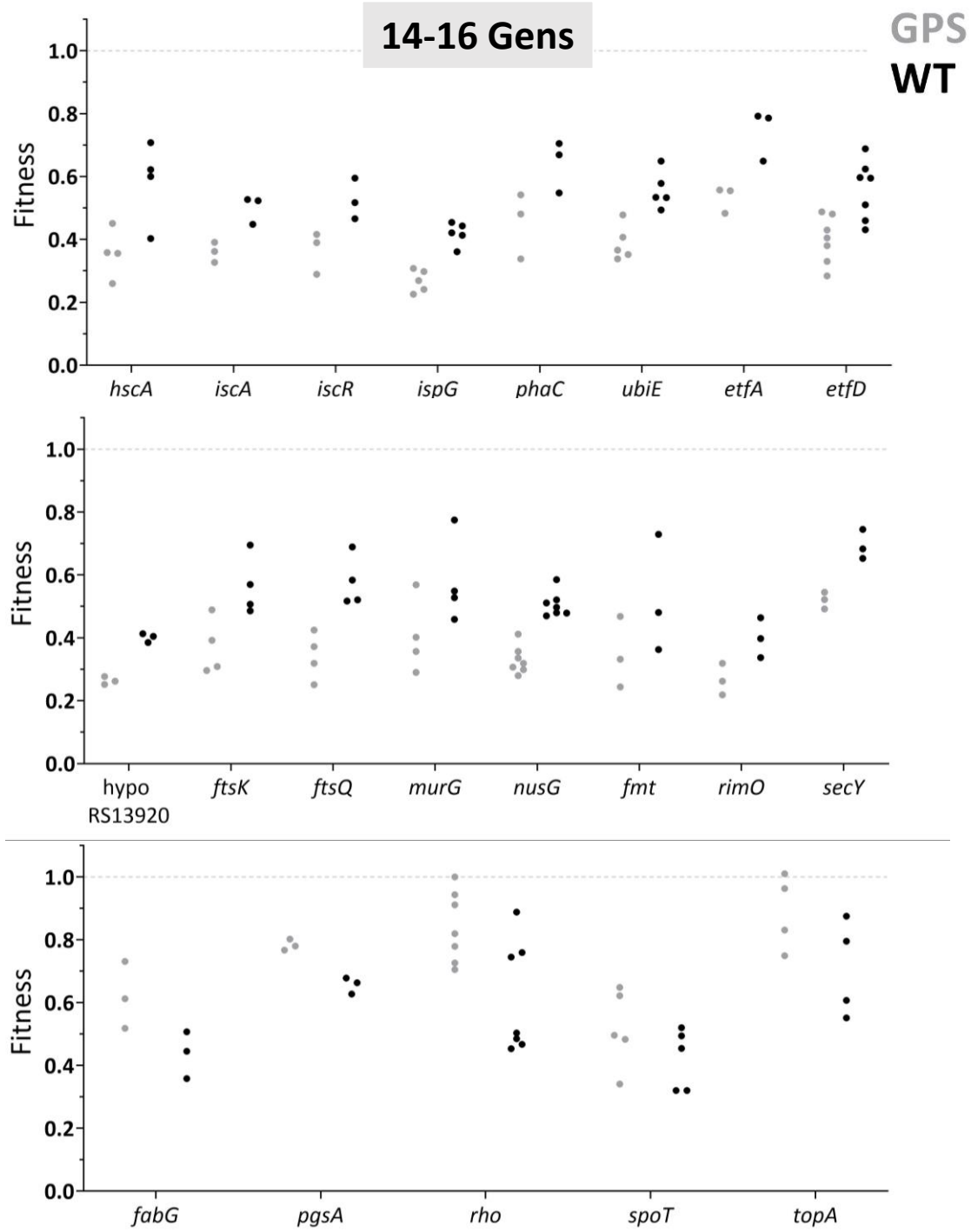
D
14-16 Gens
GPS
WT
Fitness
1.0
0.8
0.6
0.4
0.2
0.0
hscA
iscA
iscR
ispG
phaC
ubiE
etfA
etfD
hypo RS13920
ftsK
ftsQ
murG
nusG
fmt
rimO
secY
fabG
pgsA
rho
spoT
topA

Supp Fig 4

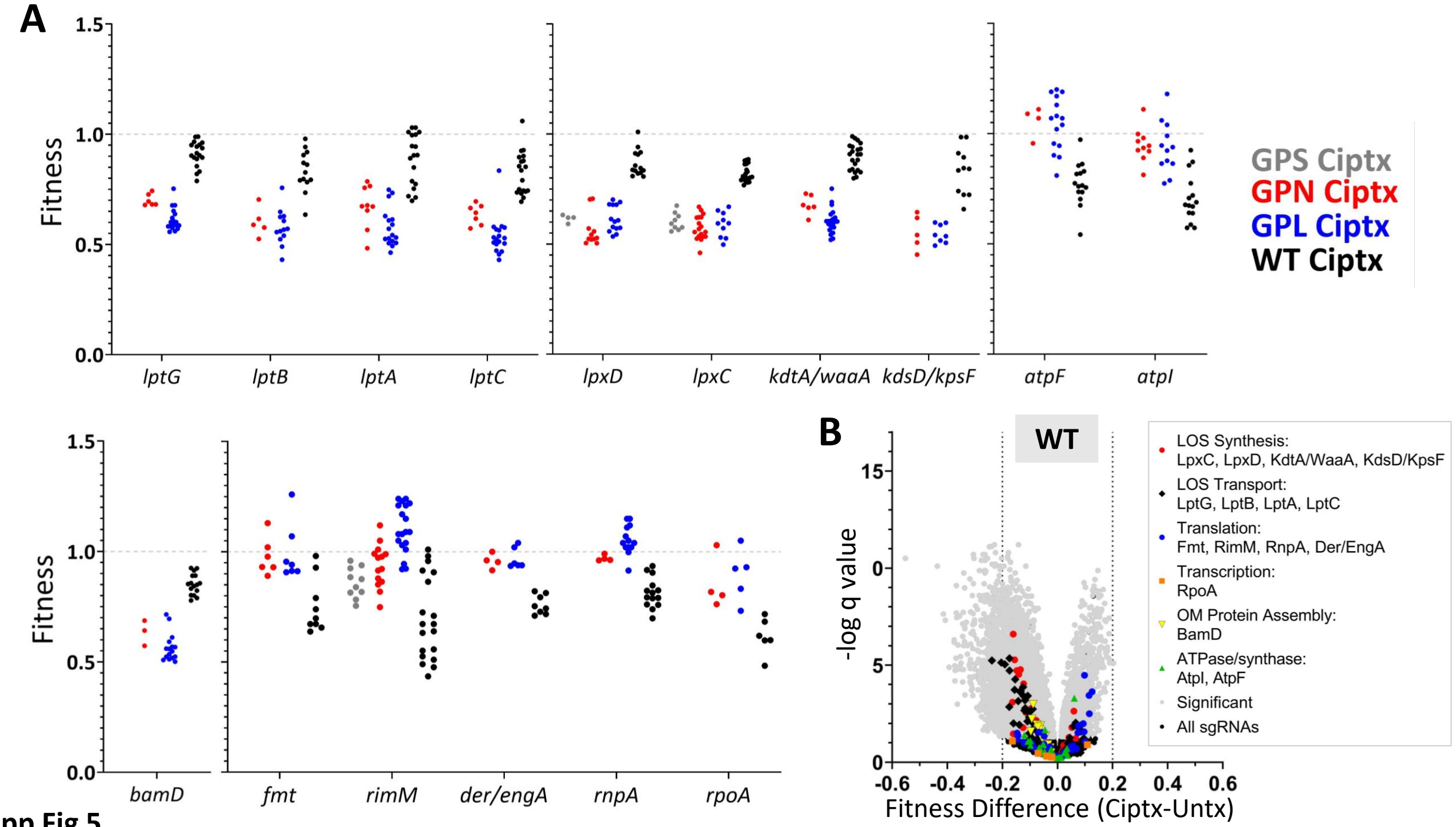
A
Fitness
1.5
1.0
0.5
0.0
lptG
lptB
lptA
lptC
lpxD
lpxC
kdtA/waaA
kdsD/kpsF
atpF
atpI
GPS Ciptx
GPN Ciptx
GPL Ciptx
WT Ciptx
bamD
fmt
rimM
der/engA
rnpA
rpoA
B
WT
-log q value
15
5
-0.6
-0.4
-0.2
0.0
0.2
0.4
0.6
Fitness Difference (Ciptx-Untx)
LOS Synthesis:
LpxC, LpxD, KdtA/WaaA, KdsD/KpsF
LOS Transport:
LptG, LptB, LptA, LptC
Translation:
Fmt, RimM, RnpA, Der/EngA
Transcription:
RpoA
OM Protein Assembly:
BamD
ATPase/synthase:
AtpI, AtpF
Significant
All sgRNAs

Supp Fig 5